U-Pb isotopic dating of columbite-tantalite minerals: Development of reference materials and in situ applications by ion microprobe

Hélène Legros, Julien Mercadier, Johan Villeneuve, Rolf Romer, Etienne Deloule, Marieke van Lichtervelde, Stijn Dewaele, Philippe Lach, Xu-Dong Che, Ru-Cheng Che, et al.

HAL Id: insu-02060870

https://insu.hal.science/insu-02060870

Submitted on 7 Mar 2019

Accepted Manuscript

U-Pb isotopic dating of columbite-tantalite minerals: Development of reference materials and in situ applications by ion microprobe

Hélène Legros, Julien Mercadier, Johan Villeneuve, Rolf L. Romer, Etienne Deloule, Marieke Van Lichtervelde, Stijn Dewaele, Philippe Lach, Xu-Dong Che, Ru-Cheng Wang, Ze-Ying Zhu, Eric Gloaguen, Jeremie Melleton
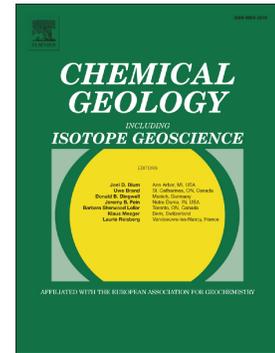
Please cite this article as: H. Legros, J. Mercadier, J. Villeneuve, et al., U-Pb isotopic dating of columbite-tantalite minerals: Development of reference materials and in situ applications by ion microprobe, Chemical Geology, https://doi.org/10.1016/j.chemgeo.2019.03.001

U-Pb isotopic dating of columbite-tantalite minerals: development of reference materials and *in situ* applications by ion microprobe

Hélène Legros [a,b,*], Julien Mercadier [a,*], Johan Villeneuve [c], Rolf L. Romer [d], Etienne Deloule [c], Marieke Van Lichtervelde [e], Stijn Dewaele [f,g], Philippe Lach [b], Xu-Dong Che [h], Ru-Cheng Wang [h]; Ze-Ying Zhu [h], Eric Gloaguen [i], Jeremie Melleton [b]

[a] *Université de Lorraine, CNRS, CREGU, GeoRessources, Boulevard des Aiguillettes B.P. 70239, F-54506 Vandoeuvre-lès-Nancy, France*

[b] *BRGM-French Geological Survey, 3, Av. Claude Guillemin, BP 36009, 45060 Orléans Cedex 2, France*

[c] *CRPG, CNRS, Université de Lorraine, UMR 7358, Vandoeuvre-les-Nancy F-54501, France*

[d] *GFZ German Research Centre for Geosciences, Telegrafenberg, 14473 Potsdam, Germany*

[e] *IRD, UR 234, GET, 14 avenue E. Belin, F-31400 Toulouse, France*

[f] *Department of Geology and Mineralogy, Royal Museum for Central Africa (RMCA), Leuvensesteenweg 13, 3080 Tervuren, Belgium*

[g] *Mineralogy and Petrology, Department of Geology, Ghent University, Krijgslaan 281 S8, 9000 Ghent, Belgium*

[h] *State Key Laboratory for Mineral Deposits Research, School of Earth Sciences and Engineering, Nanjing University, Xianlin University Town, Nanjing 210046- China*

i *Institut des Sciences de la Terre d'Orléans, CNRS, BRGM, ISTO, UMR 7327, 1A, rue de la Férollerie, 45071 Orléans cedex 2, France*

* GeoRessources UMR 7359, Université de Lorraine, Faculté des Sciences et Technologies, Entrée 3B Boulevard des Aiguillettes BP 70239, 54506 Vandoeuvre-lès-Nancy Cedex, France
Phone : +33 3 83 68 47 48

Mail : h.legros@ualberta.ca; julien.mercadier@univ-lorraine.fr

Abstract

Columbite-tantalite group minerals are the most common Nb-Ta minerals. Columbite-tantalite is particularly suitable for U-Pb dating due to its high U and low common Pb contents. *In situ* isotopic dating of columbite-tantalite by LA-ICP-MS or SIMS requires certified reference material to properly account for potential matrix effects linked to substitutions between Nb and Ta and between Mn and Fe. Our study has two objectives: i) establish a database of reference materials for *in situ* U-Pb isotopic dating of columbite-tantalite minerals and ii) test the capability of SIMS to *in situ* U-Pb date columbite-tantalite minerals of different chemical composition. Tests of *in situ* U-Pb dating demonstrate that SIMS can easily be used to date columbite-tantalite minerals with errors and precisions overlapping the reference ID-TIMS age. There are, however, significant matrix effects for non-matching Nb-Ta-Fe-Mn compositions of sample and reference material. Matrix effects are highly correlated with the Ta/(Ta+Nb) ratio of columbite-tantalite, due to the significant difference in the atomic mass of Nb and Ta. The Mn/(Mn+Fe) ratio does not significantly contribute to the observed matrix effect as the two elements have similar atomic masses. The linear correlation between Ta/(Nb+Ta) and $(({}^{206}Pb/{}^{238}U)_{SIMS}/({}^{206}Pb/{}^{238}U)_{ID\text{-}TIMS})$ obtained for columbite-tantalite minerals of known ID-TIMS age demonstrates that the SIMS matrix-effect can be properly accounted for by using the chemical composition as determined by EMPA. The ability to measure ${}^{204}Pb$ by SIMS also allows the use of reference materials with a small common lead contribution and to calculate accurate and precise ages for columbite-tantalite minerals with contributions of common lead.

Keywords

Columbite-tantalite, Niobium, Tantalum, U-Pb dating, SIMS, ID-TIMS, Geochronology

1. Introduction

Niobium and tantalum are critical resources due to their wide application in the high-tech electronics industry, in superalloys, magnets, glasses, and structural ceramics (Mineral profiles by BGS; http://www.bgs.ac.uk). Tantalum is mostly extracted from columbite-tantalite minerals $[(Fe,Mn)(Nb,Ta)_2O_6]$ that occur in rare metal granites, alkaline and carbonatitic rocks, pegmatites, and hydrothermal veins (i.e., Baumgartner et al., 2006; Mitchell 2015; Zhu et al., 2015). The improvement of exploration methods and, thus, the discovery of new niobium and tantalum deposits requires a better understanding of the geological conditions of mineralization formation. Dating columbite-tantalite mineralization provides a critical step in linking the formation of Nb and Ta resources to the tectono-metamorphic and magmatic history of an area.

Columbite-tantalite minerals have high U contents associated with low Pb_{common} contents and, thus, develop with time highly radiogenic Pb isotopic compositions (Romer and Lehmann, 1995; Romer and Smeds, 1994; Romer and Wright, 1992; Smith et al., 2004). The highly radiogenic Pb isotopic compositions allow for direct dating of these ore minerals.

Columbite-tantalite U-Pb dating by isotope dilution thermal ionization mass-spectrometry has been reported for several geological contexts (ID-TIMS; i.e. Romer and Wright, 1992; Romer and Lehmann, 1995; Romer and Smeds, 1994, 1996, 1997; Romer et al., 1996; Oberthür et al., 2002; Küster et al., 2009; Dewaele et al., 2011; Melcher et al., 2015). The high precision of ID-TIMS dating of columbite-tantalite minerals is offset by the delicate and time-consuming analytical protocol. Therefore, *in situ* techniques like laser ablation inductively-coupled plasma mass spectrometry (LA-ICP-MS) have been increasingly used over the last 15

years to date columbite-tantalite minerals (e.g., Smith et al., 2004; Dewaele et al., 2011; Gäbler et al., 2011; Melleton et al., 2012; Deng et al., 2013; Che et al., 2015; Melcher et al., 2015; Yan et al., 2016; Zhou et al., 2016; Tang et al., 2017; Van Lichtervelde et al., 2017). The results of these studies indicate that LA-ICP-MS is an appropriate method to date columbite-tantalite minerals, with less than 5% error on calculated U-Pb ratios (Che et al., 2015). Dating of columbite-tantalite minerals by Secondary Ion Mass Spectrometer (SIMS) has not been reported up to date, although this technique is considered as state-of-the-art for *in situ* U-Pb dating of minerals, with high spatial resolution (15 to 20 μm in diameter, several nm in depth) and capability to measure and, therefore, correct potential common lead contributions. The major limitation for *in situ* U-Pb isotopic dating of minerals, both by LA-ICP-MS or SIMS, is the availability of certified reference material of identical chemical composition to avoid matrix effects, which would result in inaccurate U-Pb age. Matrix effects may be particularly important for columbite-tantalite minerals that include four different chemical end members, linked to substitutions between the four main elements: Nb-Ta and Fe-Mn. The substitution of Nb (93) and Ta (180), which have very different atomic masses, may produce a significant matrix effect, whereas the substitution of Mn and Fe (55 and 56, respectively) may be less critical. Furthermore, there is a wide range of coupled substitutions, including Ti, Sn, W, Sc, and REE (e.g., Melcher et al., 2015, 2017; Müller et al., 2017). Thus, the wide range of chemical compositions of columbite-tantalite minerals may strongly affect the accuracy and quality of *in situ* U-Pb dating if no adequate chemical standards are available. Studies based on ID-TIMS have demonstrated that columbite-tantalite may have significant common lead contribution in sulfide and feldspar inclusions and metamict domains (e.g., Romer and Wright, 1992; Romer and Smeds, 1996, 1997; Müller et al., 2017), which could also represent a major drawback for *in situ* dating if not taken into account or corrected.

At present, there is no certified reference material available for SIMS and LA-ICP-MS analysis that covers the compositional range of columbite-tantalite minerals. The first applications of LA-ICP-MS for dating columbite-tantalite used non-matrix matched minerals like zircon or monazite (i.e., Smith et al., 2004; Melleton et al., 2012). During the last years, a ferrocolumbite named Coltan139 has been used for standardization of columbite-tantalite minerals of variable chemical compositions (Gäbler et al., 2011; Melcher et al., 2015; Che et al., 2015). Che et al. (2015) suggested that there are no significant matrix effects in U-Pb dating columbite-tantalite minerals of different chemical composition using LA-ICP-MS and Coltan139. Melcher et al. (2015) demonstrated that some samples, analyzed by both ID-TIMS and LA-ICP-MS methods, show inconsistent results.

This study has two objectives; (1) Develop columbite-tantalite reference material suitable for *in situ* U-Pb dating. Several columbite-tantalite samples from deposits of contrasting age have been collected, characterized by SEM and EMPA, and dated by SIMS and ID-TIMS using established analytical protocols. (2) Test the applicability and capability of state-of-the-art CAMECA IMS1270 SIMS for the dating of columbite-tantalite minerals. With this in mind, we determine U-Pb ID-TIMS ages of nine columbite-tantalite minerals and used these mienrals as reference material (i) to characterize matrix effects based on the chemical composition of columbite-tantalite minerals, (ii) to propose a procedure to correct for matrix effects, and (iii) to document the effect of non-corrected common lead contributions.

2. Sample location

At the beginning of this study, twenty-two samples from different locations were tested for chemical and isotopic homogeneity (SEM, EPMA, and SIMS analyses). The aim was to provide homogeneous (minimum at mm scale) samples, covering the entire range of chemical

composition of columbite-tantalite minerals, for U-Pb ID-TIMS dating. These samples were selected to represent various locations and geological periods. Based on these screening tests, ten samples of the original set of twenty-two samples were selected for U-Pb ID-TIMS dating. They are presented below.

2.1 CT and ISSIA samples (Ivory Coast)

These columbite-tantalite samples were collected from placers in central-west Ivory Coast that are directly associated with the weathering of local granites and pegmatites. Our samples were taken near the Issia granite, described as a non-oriented muscovite-dominated porphyroid peraluminous granite with associated Nb-Ta-Be-Li pegmatites (Allou et al., 2005).

2.2 Rongi and Buranga samples (Rwanda)

The Rongi and Buranga samples originated from two concentrates obtained by ground sluicing from pegmatites of the Karagwe-Ankole belt of Central Africa. The pegmatite fields are located near Gatumba, 50 km west of Kigali and hosted in dolerites. Details on the mineralogical assemblage of the pegmatites have been presented by Dewaele et al. (2011) and Melcher et al. (2015). The Rongi and Buranga samples were dated by TIMS at 931.1 ± 1.2 Ma (MSWD = 2.0) and 936 ± 14 Ma (MSWD = 2.5), respectively, by Melcher et al. (2015) and Dewaele et al. (2011). The chemical composition of the dated columbite-tantalite from Buranga and Rongi samples were not given by Dewaele et al. (2011), it is not clear if the dated samples belong to the same columbite-tantalite generation as the one studied here. Although the sampled pegmatite fields are considered as hosting contemporaneous

pegmatites, the two concentrates could contain columbite-tantalite minerals from pegmatites having different ages.

2.3 NT-2 sample (Shanxi Province, China)

NT-2 was sampled from the No.239 pegmatite dike from the Dahe pegmatite district. This pegmatite is located in the eastern section of the Eastern Qinling in Shangnan County, Shanxi Province, China. This sample has been already dated by LA-ICP-MS by Che et al. (2015) and yielded an age of 357 ± 5 Ma (scan) and 363 ± 4 Ma (spot) (SNNT sample in Che et al., 2015).

2.4 A-1 sample (Xinjiang Province, China)

This sample was collected near Koktokay in the Altaides and was found in the most differentiated intrusions among more than ten thousand pegmatites in the area. Petrographic details are given in Zhang et al. (2004) and Wang et al. (2012). A-1 columbite-tantalite was sampled from the same pegmatite field as sample 713-79 of Che et al. (2015) that yielded an age of 218 ± 2 Ma by LA-ICP-MS.

2.5 NP2 (Fujian, China)

NP2 was sampled from the Nanping No. 31 pegmatite. This pegmatite is located in the Northern Fujian Province, about 8 km to the west of the city of Nanping. The evolved No. 31 pegmatite shows Nb, Ta, and Sn mineralization. Petrographic details are given in Rao et al. (2009). LA-ICP-MS dating yielded a weighted $^{206}Pb/^{238}U$ age of 387.1 ± 4 Ma (Tang et al.

(2017). The sample of columbite-tantalite described in that publication is slightly richer in niobium than our sample.

2.6 CC1716 (Epesses, France)

The CC1716 sample was collected from the Variscan Epesses granite located in Vendée, not far from the cities of Châteaumur and Châteliers. Several granitic facies have been described in the sampling area (Guérangé et al., 1971) and all contain disseminated columbite-tantalite.

3. Analytical techniques

The original twenty-two columbite-tantalite samples were characterized by several steps starting with optical and electron microscopy, followed by chemical and isotopic characterization by EMPA and SIMS. Samples that are chemically heterogeneous or have fine-dispersed inclusions (e.g., feldspar) were eliminated from the sample set. Samples potentially suited as reference material eventually were U-Pb dated by ID-TIMS.

3.1 Petrographic observations by optical and electron microscopies

Petrographic images were obtained from observations of polished sections using reflected light microscopy and a HITACHI FEG S4800 scanning electron microscope (SEM) equipped with an energy dispersive spectrometer (EDS), using a Si(Li) semiconductor detector. SEM observations were done at SCMEM (Service Commun de Microscopies Electroniques et de Microanalyses) of GeoRessources laboratory (Vandoeuvre-lès-Nancy, France).

3.2 EMPA

Electron microprobe analyses (EMPA) were performed on columbite-tantalite samples for Ti, Mn, Fe, Nb, Sn, Zr, Ta, W, Pb, Th, U using a CAMECA SX100 instrument equipped with wavelength dispersive spectrometers (WDS) and calibrated using natural and synthetic oxides ($MnTiO_3$, Fe_2O_3, $LiNbO_3$, cassiterite, zircon, $LiTaO_3$, scheelite, galena, ThO_2, UO_2). The analytical conditions were: current of 20 nA and accelerating voltage of 20 kV (20kV and 100nA for Pb, U, and Th) and a counting time of 10 s per element. Total Fe is presented as FeO. Tungsten, Pb, Th, and U were systematically below the limit of detection (1 wt.%, 0.5 wt.%, 0.5 wt.% and 0.2 wt.% respectively) and are not shown in the EMPA results (Table 1, Appendix A).

3.3 SIMS

Two types of SIMS experiments were run at the CRPG-CNRS (Centre de Recherches Pétrographiques et Géochimiques, Vandoeuvre-lès-Nancy, France) using a Cameca IMS1270 ion microprobe, i.e., (i) a screening experiment to identify material that is spatially isotopically homogenous at the spot size of SIMS analysis (~15 μm) to select samples for the U-Pb ID-TIMS analysis, and (ii) U-Pb dating of columbite-tantalite minerals using reference materials of known ID-TIMS age. The analytical conditions for the screening experiment (step 1) is a simplified version of the setup applied for U-Pb dating (step 2), which is based on a method proposed by Deloule et al. (2002) and adapted from the initial protocol developed by Compston et al. (1984) for the U-Pb and Pb-Pb datings of zircons by SIMS.

The O^- primary ion beam was accelerated at 13 kV, with an intensity of 20 nA. The aperture illumination beam mode (Kohler illumination) was used with a 200 μm aperture and 15x15

μm^2 spot size. Positive secondary ions were extracted by a 10 kV potential and the spectrometer slits set for a MRP of 13000 to separate isobaric interferences on the ^{204}Pb isotope. The field aperture was set to 3,000 μm, and the transfer optic magnification adjusted to 80. Rectangular lenses were activated in the secondary ion optics to improve the transmission at high mass resolution (de Chambost et al., 1996). The energy window was opened at 30 eV, and its low energy side was positioned at 5 eV before the maximum value for the ion counting. In the ion-counting mode, a single collector mode was used, and the spectrum was scanned by peak jumping using the axial Faraday cup (FC) and the axial electron multiplier (EM).

(i) The objective of the screening experiment was to spatially randomly measure on the surface of the selected crystals the counts for ^{204}Pb, ^{206}Pb, ^{207}Pb, ^{208}Pb, and ^{238}U and the related ^{206}Pb/^{238}U, ^{207}Pb/^{235}U, and ^{207}Pb/^{206}Pb ratios to determine if the number of counts and/or the isotopic ratios vary at the spatial scale of the tested minerals (several mms). This simple screening did not involve calibration against a standard. The only purpose of this screening was to assure that the sample was isotopically homogeneous − and, thus, suitable as reference material − before taking the effort to determine its U-Pb age by ID-TIMS. The results from these preliminary tests are not included in this study.

(ii) Each analysis for U-Pb dating (step 2) consists of 10 successive cycles. Each cycle starts with the measurement of the Faraday cup background on mass 195.8 (measurement time: 4s) and the reference mass ^{181}TaO (4s, FC), the electron multiplier background on mass 203.5 (4s, EM), ^{93}Nb$_2$O (4s, FC), and the sequence ^{204}Pb (8s), ^{206}Pb (4s), ^{207}Pb (4s), ^{208}Pb (12s), ^{238}U (6s), ^{232}ThO (8s), ^{238}UO (8s) and ^{238}UO$_2$ (3s) on the EM. Potential contribution of Hg on ^{204}Pb was checked prior measurement by monitoring the mass 202. The counts on 202 were below the background value indicating absence of Hg. The background values during our analytical sessions were 0.03 cps and 13,000 cps for EM and FC respectively. A ^{238}U/^{235}U ratio of

137.88 was used to calculate the $^{207}Pb/^{235}U$ ratios based on the measured $^{206}Pb/^{238}U$ and $^{207}Pb/^{206}Pb$ ratios.

Between the measurements of two masses, a waiting time of 1 or 2 s was used. Mass and energy calibrations were checked before each measurement, after a 2 min pre-sputtering on a 20x20 μm^2 raster to clean the surface from coating and contamination. Initial data treatment, standardization against selected reference materials, calculations of U/Pb, Th/Pb and Pb/Pb ratios and related ages, and calculation of errors were done using the CAMECA SIMS data processing software and an in-house Excel spreadsheet at CRPG and used for all peer-reviewed publications based on U-Pb SIMS analyses of zircon, monazite, or uranium oxides since more than 25 years. The intensities measured for the selected isotopes are firstly background substracted and corrected from dead time of the EM (^{204}Pb, ^{206}Pb, ^{207}Pb, ^{208}Pb, ^{238}U, ^{232}ThO, ^{238}UO and $^{238}UO_2$) before calculation of the U/Pb, Th/Pb and Pb/Pb ratios and related errors using the CAMECA SIMS data processing software. Error calculation and error propagation assessment are based on the equations given by Compston et al. (1984) and Fayek et al. (2000). Instrumental fractionation on Pb isotopes is corrected based on the comparison between the $^{207}Pb/^{206}Pb$ ratios measured by SIMS and ID-TIMS for a columbite-tantalite reference materials devoided of common lead. Pb/U calibration was done based on the linear relationship between $^{238}U^{16}O/^{238}U$ and $^{206}Pb/^{238}U$ ratios for the different samples tested (Compston et al., 1984). Uncertainties for Pb-U and Pb/Pb ratios and related ages are reported at the 1σ level (Appendix B). Concordia ages and MSWD are calculated using ISOPLOT (Ludwig, 2007). Common Pb corrections are systematically applied and based on the measured ^{204}Pb content (corrected from background and dead time of the EM detector) and on the Pb isotope composition calculated from Stacey and Kramers (1975), for the ID-TIMS age of columbite-tantalite crystallization. Such a procedure allows for subtracting the

common lead contributions to ^{206}Pb and ^{207}Pb and, therefore, calculating corrected ^{207}Pb/^{206}Pb, ^{206}Pb/^{238}U, and ^{207}Pb/^{235}U ages (see Appendix B).

3.4 ID-TIMS

The U and Pb concentrations and the U-Pb isotopic ratios of columbite-tantalite were analysed at GFZ German Research Centre for Geosciences (Potsdam), using the analytical procedure described in Romer and Smeds (1996). Samples were crushed and picked under the binocular microscope. Small fragments were preferred to minimize the risk of mantled U-rich nano-inclusions and to increase the chance to selectively dissolve metamict sections, fractures filled with quartz or feldspar, and sulphide inclusions. All grains were leached in 20% HF (20 min), 6N HCl (30 min), 7N HNO$_3$ (15 min) at 70 °C and then rinsed in H$_2$O and acetone for a few minutes. All grains were then inspected under the binocular microscope to select the best grains. Treated columbite-tantalite minerals show a metallic luster. Incomplete dissolution of metamict domains typically resulted in a rusty stain. These grains were removed from the sample. A ^{205}Pb-^{235}U tracer was added before dissolving grains (mass between 0.1 mg and 0.5 mg) in 40% HF on a hot plate overnight. Lead and U were separated by ion exchange chemistry (Romer et al., 2005). Lead and U were loaded on single Re-filaments with H$_3$PO$_4$ and silica gel. Isotopic ratios of Pb and U were analysed on a Triton thermal ionization mass spectrometer (TIMS) using static multi-collection using Faraday cups or an ion counter for ^{204}Pb. Data reduction, including 0.1 % / AMU mass fractionation, U and Pb blanks, and tracer contributions, was performed as described in Schmid et al. (2003). The Th contents were calculated using the U contents, the age of the sample, and ^{208}Pb$_{rad}$/^{206}Pb$_{rad}$. Data are presented in Table 2. Uncertainties are given at the 2σ level. Data were plotted using ISOPLOT v.3.75 (Ludwig 1993).

4. Results

4.1 Optical microscopy and BSE imaging

Investigation of chips of the different selected samples using reflected light (not presented here), BSE imaging, and qualitative energy dispersive spectrometry show that the selected materials are commonly homogeneous at the millimeter scale and generally almost free of inclusions (down to the scale of tens of nm). Inclusions at the micrometer scale were observed very sporadically in CT1, ISSIA2, Rongi, and CC1716. Most inclusions (mainly feldspar and quartz) are located in fractures. Most detected inclusions are located in fractures and can be easily avoided (by selective dissolution for the ID-TIMS measurements or by the spatial resolution of the SIMS measurements). No Ta-Nb zoning was observed, except for sample CC1716.

4.2 EMPA geochemistry

On the 10 columbite-tantalite samples with homogeneous BSE, a total of 232 EMPA analyses were performed (Table 1, Appendix A), including transects for each sample. The results are plotted in the reference columbite-tantalite diagram (Fig. 1). All samples are chemically homogeneous at the different scales tested (μm to mm).

Four groups can be distinguished according to the chemical composition. Group I includes samples CT1, CT3, and CT4 and shows compositions within the ferrotapiolite field with Ta# (Ta/(Nb+Ta)) between 0.90 and 0.95 and Mn# (Mn/(Fe+Mn)) between 0.04 and 0.07.

Group II includes samples NP2 and NT-2. This group shows intermediate compositions near the miscibility gap (Fig. 1). NP2 yields Ta# between 0.50 and 0.53 and Mn# between 0.35 and 0.40, whereas NT-2 has Ta# between 0.48 and 0.50 and Mn# between 0.37 and 0.39. One analysis of NP2 shows a higher Mn# of 0.48 (Fig. 1).

Group III samples (ISSIA2 and A-1) plot in the manganotantalite field. ISSIA2 composition falls near the miscibility gap, with Ta# between 0.73 and 0.86 and Mn # between 0.57 and 0.63, whereas A-1 has higher Mn content (Mn# between 0.81 and 0.84) and lower Ta contents (Ta# between 0.69 and 0.71).

Group IV samples (Rongi, Buranga, and CC1716) plot in the ferrocolumbite field. Rongi samples are grouped at Ta# between 0.16 and 0.18 and Mn # between 0.28 and 0.34. Buranga samples display moderate Mn contents with Mn# between 0.46 and 0.49, whereas CC1716 samples show low Ta with Ta# between 0.06 and 0.11.

4.3 U-Pb ID-TIMS dating

Columbite-tantalite minerals commonly have a broad range of U contents that may reach several thousand ppm and may substitute for Fe and Mn into the crystal lattice, but for high U contents may form phases of its own (e.g., uraninite; cf. Romer et al., 1996). Furthermore, columbite-tantalite minerals typically have very low common Pb contents (except if inclusion of Pb-rich phases), as Pb is too large to substitute readily into the crystal lattice, and generally very low Th contents. The high U/Pb ratios result with time in highly radiogenic Pb isotopic compositions that allow for accurate and precise U-Pb dating (e.g., Romer and Wright, 1992; Romer and Smeds, 1994, 1996). High U contents of some columbite-tantalite minerals, however, are problematic for older samples that become increasingly metamict, which allows for loss of radiogenic Pb and introduction of mostly common Pb. If U is heterogeneously

distributed, some parts of the grain may become metamict and whereas other parts are still intact (cf. Romer and Smeds, 1996; Romer, 2003). Selective dissolution of the metamict domains eventually results in concordant ID-TIMS U-Pb data. Selective dissolution also removes inclusions of sulfides or quartz-feldspar fracture fillings that may host significant amounts of common Pb (cf. Romer and Smeds, 1996; Romer, 2003). Incomplete dissolution of metamict domains or crystallization of secondary minerals in the metamict zone may partition U and Pb and result in variably reverse and normal discordant data (see Romer et al., 2007). For LA-ICP-MS and SIMS dating, such a selective removal of inclusions and metamict segments is not performed. Instead, enhanced common Pb contents (based on the monitoring of ^{204}Pb or ^{208}Pb and of ^{206}Pb/^{204}Pb or ^{208}Pb/^{204}Pb ratios) may be used as exclusion criteria as both inclusions and variably metamict zones have high common Pb.

4.3.1 CT1 (Ivory Coast)

In a ^{206}Pb/^{238}U vs. ^{207}Pb/^{235}U diagram, all data obtained from fragments of CT1 ferrotapiolite are concordant or very close to the concordia (Fig. 2a). Two fragments only are displaced along the discordia (fragments 1 and 7). Six fragments yield an ^{207}Pb/^{206}Pb age of 2046.8 ± 1.1 Ma (2σ, MSWD = 2.2).

The different fragments have homogeneous U contents of 199 ± 12 ppm (2σ) and Pb contents with an average of 72 ± 5.4 ppm (2σ), excluding fragment 4 for Pb. Fragment 4 has a much higher Pb content (314 ppm) and a lower measured ^{206}Pb/^{204}Pb ratio due to common lead that is likely to be bound to an inclusion. Measured ^{206}Pb/^{204}Pb ratios of the remaining samples range from 1100 to 47700, implying that leaching did not completely remove inclusions hosting common lead in all fragments. The ^{207}Pb/^{206}Pb ratios are homogeneous at 0.126 ± 0.002 (2σ).

4.3.2 CT3 (Ivory Coast)

In a $^{206}Pb/^{238}U$ vs. $^{207}Pb/^{235}U$ diagram, all data from the CT3 ferrotapiolite are concordant or very close to the concordia (Fig. 2b). One fragment is discordant (fragment 9) and plots above the concordia. Six fragments yield a ^{207}Pb-^{206}Pb age of 2053.2 ± 1.3 Ma (2σ, MSWD = 2.2). The leached fragments have relatively homogeneous U (294 to 321 ppm) and Pb (107 to 118 ppm) contents, Pb showing variable but low contributions of common lead (0.08 to 2.40 ppm), which explains the large range of $^{206}Pb/^{204}Pb$ ratios (2770 to 83700). The $^{207}Pb/^{206}Pb$ ratios are homogeneous at 0.127 ± 0.0002 (2σ).

4.3.3 CT4 (Ivory Coast)

In a $^{206}Pb/^{238}U$ vs. $^{207}Pb/^{235}U$ diagram, all data (except fragment 14) from ferrotapiolite CT4 are sub-concordant (Fig. 2c). Five fragments yield a ^{207}Pb-^{206}Pb age of 2044 ± 1.6 Ma (2σ, MSWD = 1.6).

The fragments have homogeneous U (169 to 181 ppm) and Pb contents (62 to 68 ppm) with variable calculated contents of common lead (0.3 to 4.2 ppm). The large range of common lead accounts for the range in $^{206}Pb/^{204}Pb$ ratios (910 to 11100). All fragments are clustered except for fragment 14 that shows elevated common lead (4.2 ppm). The $^{207}Pb/^{206}Pb$ ratios are homogeneous at 0.126 ± 0.0001 (1σ).

4.3.4 ISSIA2 (Ivory Coast)

The fragments have highly variable U and Pb contents (172 to 990 ppm and 10 to 469 ppm respectively). Measured $^{206}Pb/^{204}Pb$ ratios are relatively low, (141 to 1290), largely due to the high calculated common Pb content that range from 2 to 17 ppm.

In a $^{206}Pb/^{238}U$ *vs.* $^{207}Pb/^{235}U$ diagram, two fragments (57 and 59) are sub-concordant and three fragments (samples 56, 58 and 60) are strongly discordant, close to the origin of the diagram (Fig. 2d). Together, these samples define a scattered Discordia (MSWD = 502) that intersects at 2002 ± 32 Ma (2σ). The high and variable U contents of the leached columbite-tantalite fragments strongly indicate that these 2 Ga old minerals are variably metamict, which is in line with the high common Pb content and the excess scatter of the Discordia (e.g., Romer, 2003; Müller et al., 2017), but also the poor metallic aspect of grains after the leaching procedure. Metamictization allows lead to migrate within the damaged zones, accounting for the very high MSWD and possibly also the slightly lower intercept age.

4.3.5 Rongi (Rwanda)

In a $^{206}Pb/^{238}U$ vs. $^{207}Pb/^{235}U$ diagram, the fragments from the Rongi ferrocolumbite are concordant (Fig. 3a), discordant (fragment 19), or are dominated by common Pb (fragments 20, 22, and 25). The four sub-concordant fragments yield a discordia age of 931.5 ± 2.5 Ma (2σ; forced through the origin of the diagram) with a very low MSWD of 0.82.

The fragments have low and variable U and Pb contents of 60 to 100 ppm and 8.25 to 14.8 ppm, respectively. Samples with very low $^{206}Pb/^{204}Pb$ values have considerably higher Pb contents (up to 236 ppm), which possibly reflects sulphide micro-inclusions that were shielded during leaching and remained in the sample.

4.3.6 Buranga (Rwanda)

In a $^{206}Pb/^{238}U$ vs. $^{207}Pb/^{235}U$ diagram, four fragments from the Buranga ferrocolumbite are concordant and one sample is discordant (41; Fig. 3b). The four fragments yield an age of 905.2 ± 3.2 Ma (2σ, MSWD = 0.41).

The fragments have rather homogeneous U and Pb contents of 74 to 84 ppm (excluding one fragment rich in common lead having 163 ppm U) and 10 to 12 ppm (excluding one fragment rich in common lead having 76.5 ppm Pb), respectively, with a variable calculated common lead contribution from 0.1 to 3.7 ppm (one fragment is rich in common lead with 56 ppm common Pb). Overall, the common lead contribution is lower than in other samples of this study. Two fragments (fragments 36 and 38), however, have high common lead contributions, but also higher contents in U, which indicates that the high common Pb may not be related to micro-inclusions, but instead may reflect common Pb that became incorporated in metamict domains. Fragments 36 and 38 were not used in age calculations.

4.3.7 NT-2 (Shanxi, China)

In a $^{206}Pb/^{238}U$ vs. $^{207}Pb/^{235}U$ diagram, six fragments from the NT-2 ferrotantalite straddle along the concordia and fall on a common discordia that does not yield a clear intercept with the concordia. The most robust age is the $^{207}Pb/^{206}Pb$ age of 372.0 ± 2.3 Ma (2σ, MSWD = 2.1), omitting fragment 48 that has a slightly older $^{207}Pb/^{206}Pb$ age (Fig. 3c).

The fragments have variable U contents from 142 to 218 ppm and low Pb content from 9 to 13 ppm, except for one fragment (46) that has a high common Pb content and, therefore, a low $^{206}Pb/^{204}Pb$ value. Calculated common Pb content of fragment (46) is 28 ppm, the other fragments have 0.7 to 1.8 ppm common Pb.

4.3.8 A-1 (Xinjiang, China)

In a $^{206}Pb/^{238}U$ vs. $^{207}Pb/^{235}U$ diagram, three fragments of manganotantalite A-1 (49, 50, 55) give a concordant age of 198.3 ± 1.4 Ma (2σ, MSWD = 0.16). Additional four fragments (51, 52, 53, and 54) are reversely discordant and fall together with the concordant samples on a discordia through the origin of the diagram (Fig. 3d). The reverse discordance seems to be an artefact from leaching.

The fragments have variable contents in U (42 to 515 ppm) and Pb (3 to 18 ppm) with variable but not excessive contribution of common lead (0.5 to 2.5 ppm). There is no correlation between U contents (of the leached fragments) and reverse discordance. The variable and in part high U contents may indicate that the untreated columbite-tantalite may have had even higher U contents, possibly resulting in local metamictization. The small variation in calculated Th/U (0.0072 ± 0.0014; 2σ) suggests that the high U contents were not related to uraninite inclusions, but were hosted in the crystal lattice.

4.3.9 NP2 (Fujian, China)

In a $^{206}Pb/^{238}U$ vs. $^{207}Pb/^{235}U$ diagram, four fragments from the NP2 ferrotantalite are concordant (27, 28, 33, 34) and two fragments are discordant (samples 31 and 30). Together, these six fragments define a discordia that passes through the origin of the diagram and yields a discordia age of 380.3 ± 2.4 Ma (2σ, MSWD = 0.9; Fig. 3e). Additional two samples with markedly deviating apparent $^{207}Pb/^{206}Pb$ ages do not fall on the discordia.

The fragments have variable U contents from 136 to 322 ppm. Lead contents are less variable and low from 12 to 16 ppm with low calculated common lead contributions (0.5 to 1.5 ppm).

4.3.10 CC1716 (France)

In a ^{206}Pb/^{238}U vs. ^{207}Pb/^{235}U diagram, all fragments of ferrocolumbite CC1716 define a discordia that passes through the origin of the diagram (Fig. 3f). One sample is strongly reverse discordant (61). The discordia yields an upper intercept age of 326.3 ± 0.6 Ma (2σ, MSWD = 1.2).

Ferrocolumbite CC1716 is unusual compared to the other samples because of its highly variable and in part extremely high U (10 to 54500 ppm) and Pb (24 to 2500 ppm) contents. Most of the Pb is radiogenic, as calculated common Pb ranges from 0.1 to 26 ppm. This sample shows heterogeneous rims (BSE). The extremely high U contents measured for some fragments may be bound to uraninite nano- to micro-inclusions that have not been observed on the thin sections during by SEM analyses.

4.4 U-Pb isotopic dating by SIMS and related calibration issues

4.4.1 U-Th-Pb raw measurements

A total of two hundred and four analyses have been performed by SIMS on nine samples previously dated by ID-TIMS (excluding ISSIA2 sample; Table 2). All analyses were performed during the same analytical session. For the overall session, the background was measured at 0.03 cps (EM, mass 203.5). For all samples and all measured points, ^{204}Pb (representing common lead) was measured with the EM above detection limit with values between 0.3 and 551 cps, ^{206}Pb from 1052 to 45143 cps, ^{207}Pb between 86.65 and 9450 cps , ^{208}Pb from 9.58 and 22825 cps and ^{238}U between 41.75 and 3210 cps. The calculated sensitivity for Pb and U are from 4.2 to 105 cps/ppm/nA (based on ^{206}Pb) and from 0.02 to

0.44 cps/ppm/nA respectively. The sensitivity is dependent on the chemical composition of the columbite-tantalite minerals, with a sensitivity for Pb from 12.5 to 24.1 cps/ppm/nA for ferrotapiolite and from 43.3 to 105 cps/ppm/nA for ferrocolumbite for example, and a sensitivity for U from 0.14 to 0.39 cps/ppm/nA for ferrotapiolite and from 0.09 to 0.44 cps/ppm/nA for ferrocolumbite for example.

The initial heterogeneous distribution of U within the columbite-tantalite crystals results in the variable cps measured for the ^{238}U and radiogenic lead isotopes for a given sample (Appendix B). The measured ^{206}Pb/^{238}U ratio may vary within samples (Appendix B) that have overall little radiogenic Pb due to moderate additions of common Pb, as in metamict domains (NP2, NT-2, and A-1). Extreme and outlier values (mainly corresponding to analyses presenting errors or isotopic ratios differing by more than 2 sigma from the mean calculated for all the data of the considered sample) have been removed from the calculation (3 values for CT1, 6 values for CT3, 1 value for CT4, 10 values for Buranga, 1 values for CC1716 and 3 values for NT-2; see Appendix B). The omitted analyses also commonly have higher Th contents, but also higher ^{204}Pb and ^{208}Pb counts than in normal zones and correspond to metamict zones or nano inclusions. In total, 24 measurements of 204 analyses have been removed during calculation due to the previously exposed reasons. These data are shown in italic in Appendix B.

Ferrotapiolite and ferrocolumbite samples have low ^{204}Pb contents, except for the Buranga sample, which displays a larger variability for four measurements (of thirty-five). The Rongi samples also have higher ^{208}Pb content (coupled to higher ^{204}Pb) reflecting the presence of common Pb as also inferred from the Pb isotopic composition of the ID-TIMS data (data in italic in Appendix B). Ferrotantalite and manganotantalite samples display much higher and more variable contents of common Pb. These variations Pb content may reflect metamict domains.

The $^{206}Pb/^{204}Pb$ ratios are between 6711 and 219780 for ferrotapiolite samples, between 1001 and 68493 for ferrocolumbite and between 185 and 4837 for ferrotantalite. Only one of five manganocolumbite analyses shows low common lead contribution (sample A-1), with a $^{206}Pb/^{204}Pb$ ratio of 1029. This sample is the only one of this composition; therefore, no SIMS ages could be obtained for this sample due to the lack of another sample as a matrix-matched standard. The $^{206}Pb/^{204}Pb$ ratios are variable within individual sample. The variation of the $^{206}Pb/^{204}Pb$ ratios within an individual sample is linked to the content of common lead and to the initial heterogeneous distribution of uranium, whereas the variation among different samples, in addition, reflects age differences. The values and variations of the $^{206}Pb/^{204}Pb$ ratios measured by SIMS for the different samples are comparable to those measured by ID-TIMS on different fragments of each sample.

4.4.2 Matrix effects

The U-Pb dating of minerals by SIMS requires correction for different instrumental fractionation factors for U and Pb that have different energy distributions and ionization potentials (Hinton, 1990), which affects the measured U/Pb ratios. Interelement fractionation between U and Pb for an unknown sample of a considered mineral (zircon, monazite, xenotime, titanite, uraninite or rutile for example) can be corrected by plotting and comparing the $^{206}Pb/^{238}U$ against UO/U of both sample and reference material of the same matrix (i.e. Zhu et al., 1998; Deloule et al., 2002; Valli et al., 2008; Lesbros-Piat-Desvial et al., 2017). This relation was first established by the Local Thermodynamic Equilibrium (LTE) Model of Andersen and Hinthorne (1973) which provides elemental concentration estimates for a broad range of materials. This model predicted the covariation of the Pb^+/U^+ and UO^+/U^+ ratios as

long as the sample has a constant Pb/U (Hinthorne et al., 1979). Compston et al. (1984) later proposed the correlation to be linear for the SIMS analysis of zircons.

The comparison of the raw UO/U and $^{206}Pb/^{238}U$ ratios obtained for the nine columbite-tantalite samples demonstrates that groups of different chemical composition (Fig. 1) define separate linear relations (Fig. 4a). The correlations between raw UO/U and raw $^{206}Pb/^{238}U$ ratios also depend on the age of the samples (Table 2). To account for the effect of contrasting crystallization age, the raw UO/O SIMS ratio is compared to the raw $^{206}Pb/^{238}U$ SIMS ratio divided by the $^{206}Pb/^{238}U$ ID-TIMS ratio (noted as $^{206}Pb/^{238}U_{SIMS}$ / $^{206}Pb/^{238}U_{ID-TIMS}$ thereafter). The relation between these two ratios for the different tested samples is linear (Fig. 4b) and can be expressed as:

$$^{206}Pb/^{238}U_{SIMS} / {}^{206}Pb/^{238}U_{ID-TIMS} = 8.0355 \ (UO/U) - 98.364 \ (R^2 = 0.97) \quad (1)$$

The UO/U values for the different minerals are correlated but are different, being around 16-20 for the ferrotapiolites to around 27-40 for the ferrocolumbites. Therefore, the variations in UO/U depend on the chemical composition of columbite-tantalite.

The $^{206}Pb/^{238}U_{SIMS}$ / $^{206}Pb/^{238}U_{ID-TIMS}$ ratios show a direct linear anti-correlation with the Ta/(Nb+Ta) ratio (also referred as Ta#; Fig. 5a). The anti-correlation is the following:

$$^{206}Pb/^{238}U_{SIMS} / {}^{206}Pb/^{238}U_{ID-TIMS} = -169.63 \ (Ta\#) + 206.28 \ (R^2 = 0.96) \quad (2)$$

There is no correlation between $^{206}Pb/^{238}U_{SIMS}$ / $^{206}Pb/^{238}U_{ID-TIMS}$ and Mn/(Mn+Fe) (Mn#; Fig. 5b). The anti-correlation between $^{206}Pb/^{238}U_{SIMS}$ / $^{206}Pb/^{238}U_{ID-TIMS}$ and Ta# demonstrates that SIMS analyses of columbite-tantalite minerals are affected by major matrix effects and that these effects are mainly related to the Nb-Ta exchange in columbite-tantalite group minerals. Columbite-tantalite and ferrotapiolite fall on the same trend, which indicates that the contrasting crystal structure of these minerals does not seem to have a significant effect on instrumental fractionation.

Figure 6 illustrates the analytical bias generated by these matrix effects. Figure 6a shows the $^{206}Pb/^{238}U$, $^{207}Pb/^{235}U$ and $^{207}Pb/^{206}Pb$ ages for ferrotapiolite CT3 calibrated with the matrix-matched ferrotapiolite CT1. In that case, the data are sub-concordant to concordant, and the calculated SIMS $^{206}Pb/^{238}U$ (2064 ± 6 Ma; 2σ) and $^{207}Pb/^{206}Pb$ (2055 ± 3 Ma; 2σ) ages are within uncertainties identical with the ID-TIMS ages (2059 Ma and 2053 Ma, respectively, Table 2). If ferrotapiolite CT3 is calibrated with ferrocolumbite Rongi (Fig. 6b), which has a different chemical composition, the data are discordant, and there is a significant matrix effect on the calculated apparent $^{206}Pb/^{238}U$ age (1762 ± 9 Ma; 2σ), and $^{207}Pb/^{235}U$ age (1888 ± 6 Ma; 2σ). The calculated $^{207}Pb/^{206}Pb$ age (2029 ± 3 Ma; 2σ) for non-matrix-matched conditions is slightly lower than the $^{207}Pb/^{206}Pb$ ID-TIMS (Fig. 6c). The matrix effect, and thus the deviation of SIMS $^{206}Pb/^{238}U$ and $^{207}Pb/^{235}U$ ages compared to the ID-TIMS $^{206}Pb/^{238}U$ and $^{207}Pb/^{235}U$ ages, increases linearly with the difference for the Ta# between the reference material and the columbite-tantalite crystal to date, as exemplified with the tests done on sample CC1716 (Fig. 6d).

4.4.3 Ferrotapiolite dating results (CT1, CT3, CT4)

A total of eighty-seven analyses were performed on the three samples. The results are listed in Appendix B, and the age calculation diagrams are shown in Fig. 7. Three samples of ferrotapiolite were measured: CT1, CT3, and CT4. Sample CT1 was used as an external standard to measure CT3 and CT4 U-Pb and $^{207}Pb/^{206}Pb$ isotopic ratios. Thirty-eight (out of forty-one) analyses of CT1 were used as standard values. Three measurements were discarded due to abnormally low counts on the ^{206}Pb, ^{207}Pb, and ^{238}U isotopes. Ratios have been plotted in concordia diagrams and define two discordias with concordant and sub-concordant data.

Thirty measurements (out of thirty-six) on CT3 sample define a discordia with an intercept at 2054.1 ± 2.2 Ma (2σ, MSWD = 0.95). The measurements are concordant except for three spots that are slightly discordant. The intercept age is consistent with the ID-TIMS age of 2053.2 ± 1.3 Ma. Six data have been discarded for calculation. These measurements have high Th, low Pb and/or high Nb_2O contents, possibly reflecting the presence of micro-inclusions. Nine of ten measurements from sample CT4 fall on a discordia that intercepts the concordia at 2042.0 ± 4.0 (2σ, MSWD = 0.55). One measurement falls on the concordia, whereas the nine others are sub-concordant and plot above the concordia. This age matches the ID-TIMS measurements that yielded an age of 2044.5 ± 1.6 Ma. One measurement was not included in the calculation due to anomalous thorium content (ten times more counts).

4.4.4 Ferrocolumbite dating results (Rongi, Buranga, CC1716)

A total of sixty-seven analyses were performed on three ferrocolumbite samples from Rongi, Buranga, and CC1716. The results are listed in Appendix B, and the age calculation diagrams are shown in Fig. 7. The Buranga sample was used as an external standard to calibrate and calculate the isotopic ratios of samples Rongi and CC1716. Twenty-five (out of thirty-five) measurements have been used for standardization. The omitted measurements have high common Pb, high [208]Pb and/or anomalous [206]Pb and [207]Pb contents. Both Rongi and CC1716 samples yield concordia ages.

Seventeen measurements of sample Rongi yield an age of 905.0 ± 5.0 Ma (2σ, MSWD = 0.93). Fourteen measurements (out of fifteen) of sample CC1716 yield an age of 334.6 ± 2.6 Ma (2σ, MSWD = 1.5). All data are sub-concordant. One measurement from CC1716 was discarded because of its different Ta#, indicating that this last spot was placed on the heterogeneous rim of the crystal.

4.4.5 Ferrotantalite dating results (NP2, NT-2)

A total of forty-five analyses were performed on two ferrotantalite samples: NP2 and NT-2. The results are listed in Appendix B, and the age data are shown in Fig. 7. NP2 was used as external standard to calculate the NT-2 isotopic ratios. No data was discarded from the twenty-four measurements made on the NP2 standard sample. Both samples have relatively high common lead contents and highly variable Pb ratios due to common Pb and sample heterogeneity. No inclusions were visible by reflected light or SEM (see discussion for details).

Eighteen out of twenty-one measurements of sample NT-2 are subconcordant and yield a mean $^{206}Pb/^{238}U$ age of 371.3 ± 3.7 Ma (2σ). This age is in accordance with ID-TIMS measurements (372.0 ± 2.3 Ma). Three measurements were discarded due to high common Pb or different Ta# indicating heterogeneity.

5. Discussion

5.1 Disturbances and effect on the relevance of the isotopic dating of columbite-tantalite minerals

Ten minerals were selected to be dated by ID-TIMS. Nine of them yield well-constrained ages, whereas sample ISSIA2 shows significant excess scatter and yields an age that is younger than the age of other columbite samples from the same location (CT1, CT3, CT4; Fig. 2). A possible explanation for this contrasting behavior is that this sample is strongly metamict. Selective dissolution of columbite-tantalite minerals may remove metamict

domains and result in concordant data (e.g., Lindroos et al., 1996; Romer and Smeds, 1996). This procedure, however, is not applicable for samples to be dated by SIMS. Thus, there are two questions of interest for *in situ* age determination: (i) does non-ideal behavior during leaching affect the age obtained by ID-TIMS and (ii) will the metamict nature of some domains affect *in situ* dating?

(i) Preferential removal of U or Pb during the selective dissolution of metamict domains from an initially undisturbed sample will result in discordant data. A discordia defined through these data will pass through the origin of the concordia diagram and yield the same age as the undisturbed sample. Scatter about the concordia typically is small. In contrast, a sample that had shown open-system behavior or mineral internal redistribution of U and Pb (for instance during later recrystallization) before selective dissolution will show a non-zero lower intercept age, excess scatter, and an incorrect upper intercept age, as sample ISSIA2. Anomalous leaching behavior also may be observed for minerals that experienced a redistribution of U and Pb at a scale considerably smaller than the size of the fragments used for U-Pb dating (see also Romer, 2003).

(ii) Alpha-recoil has two effects: it makes the U-hosting mineral locally metamict, and it displaces the daughter isotopes. In metamict domains, U and Pb are mobile and may become redistributed on a small scale. As long as the transport distance is much smaller than the sample size, the system appears as a closed system. Interconnected metamict domains may allow for the migration of U and Pb over longer distances. Thereby, Pb and/or U may be lost from the mineral. Metamict domains are also prone to additions of material as instance Ca or common Pb (cf. Geisler et al., 2001, 2002; Romer, 2003). Thus, metamict sections may have enhanced ^{204}Pb contents. As samples used for SIMS dating are not treated by selective dissolution, SIMS data may show higher ^{204}Pb contributions than ID-TIMS data from corresponding samples that had been leached. In minerals with heterogeneous U distribution,

☐-recoil eventually results in a Pb excess in those zones that have low U content and a Pb deficit in domains with high U content (cf. Romer, 2003). Columbite-tantalite minerals with uraninite inclusions could have such local excess of radiogenic Pb and may yield too old $^{206}Pb/^{238}U$ ages for SIMS analysis in comparison with bulk ID-TIMS ages. Such a situation may apply to sample CC1716 that has very variable average U contents in columbite fragments, some of them even higher than 1 wt. % U (Table 2). Samples with heterogeneous U distribution, however, are not suitable to be used as reference material for U-Pb dating.

5.2 Matrix effects linked to Nb/Ta composition, identification by SIMS and correction

Our results demonstrate major matrix effects for U-Pb SIMS dating of columbite-tantalite minerals (Fig. 4, 5 and 6). These matrix effects correlate with the Ta/(Nb+Ta) ratio of the columbite-tantalite minerals, whereas the Mn/(Fe+Mn) ratio does not significantly affect the determination of U/Pb isotope ratios by SIMS (Fig. 5 and 6). The measured matrix effects reflect the difference in atomic mass between the substituting elements Nb (93) and Ta (180). Such a large difference does not exist for Mn and Fe (atomic masses of 55 and 56, respectively). It this therefore essential to determine the chemical composition of columbite-tantalite minerals by EMPA before SIMS dating to use the appropriate reference material. Based on the linear calibration established between Ta# of columbite-tantalite minerals and the matrix effect (Fig. Fig. 4b and 5), the Pb/U ages of a undated columbite-tantalite can be estimated even if there is no reference material with an equivalent Ta# available, by using two reference materials of contrasting chemical compositions to bracket the composition of the unknown sample and by measuring the Ta# of the undated sample. The linear correlation between $^{206}Pb/^{238}U_{SIMS}/^{206}Pb/^{238}U_{ID\text{-}TIMS}$ and Ta# for the reference materials and the undated

sample and the measurement of the $^{206}Pb/^{238}U_{SIMS}$ for reference materials and undated sample permits indeed to estimate to $^{206}Pb/^{238}U_{ID\text{-}TIMS}$ of the undated sample and thus its $^{206}Pb/^{238}U$ age (see example in Supplementary material A). A similar calculation can be done for $^{207}Pb/^{235}U$ age.

5.3 Reliability of columbite-tantalite mineral U-Pb dating by SIMS

Our results demonstrate that SIMS is an instrument suited for *in situ* U-Pb dating of columbite-tantalite minerals. The tested columbite-tantalites minerals typically have U and Pb concentrations between 40 and 1000 ppm and between 8 to 470 ppm, respectively. The calculated sensitivities based on the applied SIMS analytical setup is between 0.02 and 0.4 cps/ppm/nA for U and between 4.2 and 105 cps/ppm/nA for Pb (based on ^{206}Pb). The precision obtained by SIMS for the $^{206}Pb/^{238}U$ and $^{207}Pb/^{235}U$ ages may be as good as 0.6 % and 1.2 % for samples without common Pb (Appendix B), for a primary beam energy of 20 nA and with an analysed zone of a diameter comprised between 15 to 20 µm and a depth of a few nanometers. The $^{207}Pb/^{235}U$ ratios are far more sensitive to the presence of common lead than the $^{206}Pb/^{238}U$ ratios, resulting in the lower precision calculated for the $^{207}Pb/^{235}U$ ages.

The accuracy of SIMS age data directly depends on the match of the chemical composition of reference and sample materials. The best accuracy will be obtained if reference material and unknown have the same Nb/Ta chemical composition and similar age. Based on the dating of CT3 using CT1 as the reference (Fig. 7), the deviation between ID-TIMS and $^{206}Pb/^{238}U$ age SIMS ages may be less than 2%. The deviation between SIMS and ID-TIMS ages is > 2% for Rongi (Table 3) and is explained by the fact that SIMS and ID-TIMS dating was done on different crystals from a processed mineral concentrate. Excluding any analytical problem, it is possible that these two crystals come from two different pegmatites with different ages (931

Ma for the ID-TIMS fragment and 905 Ma for SIMS fragment). These ages agree with those of various pegmatites in the area (Melcher et al., 2015).

Most columbite-tantalite minerals have low common lead contents (Appendix B). Thus, the majority of SIMS analyses has high $^{206}Pb/^{204}Pb$ ratios, and the common Pb correction has no significant effect on the isotopic U/Pb ages. Several analyses, however, have ^{204}Pb intensity significantly above detection limit (maximum of 551 cps of ^{204}Pb), in particular, the Rongi, NP2, NT-2, A-1, and CC1716 samples. These fragments have markedly lower measured $^{206}Pb/^{204}Pb$ (x00) and $^{207}Pb/^{204}Pb$ ratios. These analyses have to be corrected for common lead contributions, as uncorrected data will yield too high $^{206}Pb/^{238}U$ and $^{207}Pb/^{235}U$ ratios and, thus, too old $^{206}Pb/^{238}U$ and $^{207}Pb/^{235}U$ ages (Fig. 8a and c). Furthermore, such data tends to fall to the right of the concordia (Fig. 8). For SIMS data, there are two options to deal with the common Pb problem: (i) use the measured ^{204}Pb to correct for common Pb (Fig. 8a and c) or (ii) use a Tera-Wasserburg diagram that allows obtaining intercept ages from uncorrected data (Fig. 8b and d).

6. Conclusion

We characterize columbite-tantalite minerals covering a significant range of compositional variation known for columbite-tantalite minerals and having ages between 198.3 ± 1.4 Ma to 2053.2 ± 1.3 Ma. The various minerals are chemically homogenous, and several among them may serve as reference materials for *in situ* U-Pb dating. The different columbite-tantalite minerals are available to the scientific community, depending of the quantity available for each reference material.

The U-Pb dating of columbite-tantalite minerals by SIMS demonstrates that there are major matrix effects that mainly depend on the Nb/Ta ratio of the columbite-tantalite minerals.

Matrix matching of unknown and reference material yields accurate and precise U-Pb ages. Our results imply that the U-Pb dating of columbite-tantalite minerals by SIMS requires either (i) a reference material with the same Nb/Ta ratio as the mineral to date or (ii) – based on the correlation between $^{206}Pb/^{238}U_{SIMS}$ / $^{206}Pb/^{238}U_{ID-TIMS}$ and Ta/(Nb+Ta) – a series of reference materials of contrasting Nb/Ta to interpolate the matrix correction of non-matching reference materials. The potential contribution of common lead, however, can be accurately detected and corrected by SIMS.

References

Allou, B.A., Lu, H.Z., Guha, J., Carignan, J., Naho, J., Pothin, K., Yobou, R., 2005. Une Corrélation Génétique entre les Roches Granitiques, et les Dépôts Éluvionnaires, Colluvionnaires et Alluvionnaires de Columbite-tantalite d'Issia, Centre-Ouest de la Côte d'Ivoire. Exploration and Mining Geology 14, 61-77. (in French)

Andersen, C., and Hinthorne, J.R., 1973. Thermodynamic approach to the quantitative interpretation of sputtered ion mass spectra. Analytical Chemistry 45, 1421-1438.

Baumgartner, R., Romer, R.L., Moritz, R., Sallet, R., Chiaradia, M., 2006. Columbite–tantalite-bearing granitic pegmatites from the Seridó Belt, northeastern Brazil: genetic constraints from U–Pb dating and Pb isotopes. The Canadian Mineralogist 44, 69-86.

Che, X.D., Wu, F.Y., Wang, R.C., Gerdes, A., Ji, W.Q., Zhao, Z.H., Yang, J.H., Zhu, Z.Y., 2015. In situ U–Pb isotopic dating of columbite–tantalite by LA–ICP–MS. Ore Geology Reviews 65, 979-989.

Compston, W., Williams, I.S., Meyer, C., 1984. U–Pb geochronology of zircons from lunar breccia 73217 using a sensitive high mass-resolution ion probe. Proceedings of the fourteenth lunar and planetary science conference,

Part 2, Journal of Geophysical research, Vol. 89, B525–B534.

De Chambost, E., Schuhmacher, M., Lovestam, G., Claesson, S., 1996. Achieving high transmission with the Cameca IMS-1270. Secondary ion mass spectrometry, SIMS X. Wiley, Chichester, 1003-1006.

Deloule, E., Alexandrov, P., Cheilletz, A., Laumonier, B., Barbey, P., 2002. In-situ U–Pb zircon ages for Early Ordovician magmatism in the eastern Pyrenees, France: the Canigou orthogneisses. International Journal of Earth Sciences 91, 398-405.

Deng, X.D., Li, J.W., Zhao, X.F., Hu, Z.C., Hu, H., Selby, D., de Souza, Z.S., 2013. U–Pb isotope and trace element analysis of columbite-(Mn) and zircon by laser ablation ICP–MS: Implications for geochronology of pegmatite and associated ore deposits. Chemical geology 344, 1-11.

Dewaele, S., Henjes-Kunst, F., Melcher, F., Sitnikova, M., Burgess, R., Gerdes, A., Fernandez, M.A., De Clercq, F., Muchez, P., Lehmann, B., 2011. Late Neoproterozoic overprinting of the cassiterite and columbite-tantalite bearing pegmatites of the Gatumba area, Rwanda (Central Africa). Journal of African Earth Sciences 61, 10-26.

Fayek, M., Harrison, T. M., Grove, M., Coath, C.D., 2000. A rapid in situ method for determining the ages of uranium oxide minerals: Evolution of the Cigar Lake deposit, Athabasca Basin. International Geology Review 42, 163-171.

Gäbler, H.E., Melcher, F., Graupner, T., Bahr, A., Sitnikova, M.A., Henjes-Kunst, F., Oberthur, T., Bratz, H., Gerdes, A., 2011. Speeding Up the Analytical Workflow for Coltan Fingerprinting by an Integrated Mineral Liberation Analysis/LA-ICP-MS Approach. Geostandards and Geoanalytical Research 35, 431-448.

Geisler, T., Ulonska, M., Schleicher, H., Pidgeon, R. T., van Bronswijk, W., 2001. Leaching and differential recrystallization of metamict zircon under experimental hydrothermal conditions. Contributions to Mineralogy and Petrology 141, 53-65.

Geisler, T., Pidgeon, R. T., Van Bronswijk, W., Kurtz, R., 2002. Transport of uranium, thorium, and lead in metamict zircon under low-temperature hydrothermal conditions. Chemical Geology 191, 141-154.

Guérangé, B., Guigues J., Moussu, R., Parfenoff, A., 1971. Un granite niobo-tantalifère : le massif des épesses (Massif Armoricain, Vendée, France). Colloque scientifique du Bureau de Recherche Géologiques et Minières, 130-138. (in French)

Hinthorne, J.R., Andersen, C.A., Conrad, R.L., Lovering, J.F., 1979. Single-grain $^{207}Pb^{206}Pb$ and U/Pb age determinations with a 10-μm spatial resolution using the ion microprobe mass analyzer (IMMA). Chemical Geology 25, 271-303.

Hinton, R.W., 1990. Ion microprobe trace-element analysis of silicates: Measurement of multi-elemental glasses. Chemical Geology 83, 11-25.

Küster, D., Romer, R.L., Tolessa, D., Zerihun, D., Bheemalingsewara, K., Melcher, F., Oberthür, T., 2009. The Kenticha rare-element pegmatite, Ethiopia: internal differentiation, U–Pb age and Ta mineralization. Mineralium Deposita 44, 723–750.

Lesbros-Piat-Desvial, M., Beaudoin, G., Mercadier, J., Creaser, R., 2017. Age and origin of uranium mineralization in the Camie River deposit (Otish Basin, Québec, Canada). Ore Geology Reviews 91, 196-215.

Lindroos, A., Romer, R.L., Ehlers, C., Alviola, R., 1996. Late-orogenic Svecofennian deformation in SW Finland constrained through pegmatite emplacement ages. Terra Nova 8, 567-574.

Ludwig, K.R., 1993. ISOPLOT: a plotting and regression program for radiogenic-isotope data. U.S. Geological Survey, Open File Report, 91–445, 1–42.

Melcher, F., Graupner, T., Gäbler, H. E., Sitnikova, M., Henjes-Kunst, F., Oberthür, T., Gerdes, A., Dewaele, S., 2015. Tantalum–(niobium–tin) mineralisation in African pegmatites and rare metal granites: Constraints from Ta–Nb oxide mineralogy, geochemistry and U–Pb geochronology. Ore Geology Reviews 64, 667-719.

Melcher, F., Graupner, T., Gäbler, H. E., Sitnikova, M., Oberthür, T., Gerdes, A., Badanina, E., Chudy, T., 2017. Mineralogical and chemical evolution of tantalum–(niobium–tin) mineralisation in pegmatites and granites. Part 2: Worldwide examples (excluding Africa) and an overview of global metallogenetic patterns. Ore Geology Reviews 89, 946-987.

Melleton, J., Gloaguen, E., Frei, D., Novák, M., Breiter, K., 2012. How are the emplacement of rare-element pegmatites, regional metamorphism and magmatism interrelated in the Moldanubian domain of the Variscan Bohemian Massif, Czech Republic? The Canadian Mineralogist 50, 1751-1773.

Mitchell, R.H., 2015. Primary and secondary niobium mineral deposits associated with carbonatites. Ore Geology Reviews 64, 626-641.

Müller, A., Romer, R.L., Pedersen, R.-B., 2017. The Sveconorwegian Pegmatite Province − thousands of pegmatites without parental granite. Canadian Mineralogist 55, 1-33.

Oberthür, T., Weiser, T.W., Gast, L., Schoenberg, R., Davis, D.W., 2002. Platinum-group minerals and other detrital components in the Karoo-age Somabula gravels, Gweru, Zimbabwe. Canadian Mineralogist 40, 435–456.

Rao, C., Wang, R.C., Hu, H., Zhang, W.L., 2009. Complex internal textures in oxide minerals from the Nanping No. 31 dyke of granitic pegmatite, Fujian Province, southeastern China. Canadian Mineralogist 47, 1195–1212.

Romer, R.L., 2003. Alpha-recoil in U-Pb geochronology: effective sample size matters. Contributions to Mineralogy and Petrology 145, 481–491.

Romer, R.L., and Lehmann, B., 1995. U-Pb columbite age of Neoproterozoic Ta-Nb mineralization in Burundi. Economic Geology 90, 2303-2309.

Romer, R.L., and Smeds, S.A., 1994. Implications of U-Pb ages of columbite-tantalites from granitic pegmatites for the Palaeoproterozoic accretion of 1.90–1.85 Ga magmatic arcs to the Baltic Shield. Precambrian Research 67, 141-158.

Romer, R.L., and Smeds, S.A., 1996. U-Pb columbite ages of pegmatites from Sveconorwegian terranes in southwestern Sweden. Precambrian Research 76, 15-30.

Romer, R.L., and Smeds, S.A., 1997. U–Pb columbite chronology of post-kinematic Palaeoproterozoic pegmatites in Sweden. Precambrian Research 82, 85–99.

Romer, R.L., and Wright, J.E., 1992. U-Pb dating of columbites: A geochronologic tool to date magmatism and ore deposits. Geochimica et Cosmochimica Acta 56, 2137-2142.

Romer, R.L., Smeds, S.A., Černý, P., 1996. Crystal-chemical and genetic controls of U-Pb systematics of columbite-tantalite. Mineralogy and Petrology 57, 243-260.

Romer, R.L., Heinrich, W., Schröder-Smeibidl, B., Meixner, A., Fischer, C.O., Schulz, C., 2005. Elemental dispersion and stable isotope fractionation during reactive fluid-flow and fluid immiscibility in the Bufa del Diente aureole, NE-Mexico: Evidence from radiographies and Li, B, Sr, Nd, and Pb isotope systematics. Contributions to Mineralogy and Petrology 149, 400-429.

Romer, R.L., Nowaczyk, N., Wirth, R., 2007. Secondary Fe-Mn-oxides in minerals heavily damaged by α-recoil: possible implications for palaeomagnetism. International Journal of Earth Science 96, 375–387.

Schmid, R., Romer, R.L., Franz, L., Oberhänsli, R., Martinotti, G., 2003. Basement-cover sequences within the UHP unit of the Dabie Shan. Journal of Metamorphic Geology 21, 531–538.

Smith, S. R., Foster, G. L., Romer, R. L., Tindle, A. G., Kelley, S. P., Noble, S. R., Horstwood, M., Breaks, F. W., 2004. U-Pb columbite-tantalite chronology of rare-element pegmatites using TIMS and Laser Ablation-Multi Collector-ICP-MS. Contributions to Mineralogy and Petrology 147, 549-564.

Stacey, J.S., and Kramers, J.D., 1975. Approximation of terrestrial lead isotope evolution by a two-stage model. Earth and Planetary Science Letters 26, 207-221.

Tang, Y., Zhao, J.Y., Zhang, H., Cai, D. W., Lv, Z.H., Liu, Y. L., Zhang, X., 2017. Precise columbite-(Fe) and zircon U-Pb dating of the Nanping No. 31 pegmatite vein in northeastern Cathaysia Block, SE China. Ore Geology Reviews 83, 300-311.

Valli, F., Leloup, P.H., Paquette, J.L., Arnaud, N., Li, H., Tapponnier, P., Lacassin, R., Guillot, S., Liu, D., Deloule, E., Xu, Z., Mahéo, G., 2008. New U-Th/Pb constraints on timing of shearing and long-term slip-rate on the Karakorum fault. Tectonics 27, doi:10.1029/2007TC002184.

Van Lichtervelde, M., Grand'Homme, A., de Saint-Blanquat, M., Olivier, P., Gerdes, A., Paquette, J.L., Melgarejo, J.C., Druguet, E., Alfonso, P., 2017. U-Pb geochronology on zircon and columbite-group minerals of the Cap de Creus pegmatites, NE Spain. Mineralogy and Petrology 111, 1-21.

Wang, R.C., Che, X.D., Zhang, W.L., Zhang, A.C., Zhang, H., 2012. Geochemical evolution and late re-equilibration of Na–Cs-rich beryl from the Koktokay #3 pegmatite (Altai, NW China). European Journal of Mineralogy 21, 795–809.

Yan, Q.H., Qiu, Z.W., Wang, H., Wang, M., Wei, X.P., Li, P., Zhang, R.Q., Li, C.Y., Liu, J.P., 2016. Age of the Dahongliutan rare metal pegmatite deposit, West Kunlun, Xinjiang (NW China): Constraints from LA–ICP–MS U–Pb dating of columbite-(Fe) and cassiterite. Ore Geology Reviews, in press.

Zhang, A.C., Wang, R.C., Hu, H., Zhang, H., Zhu, J.C., Chen, X.M., 2004. Chemical evolution of Nb–Ta oxides and zircon from the Koktokay No. 3 granitic pegmatite, Altai, northwestern China. Mineralogical Magazine 68, 739–756.

Zhou, Q., Qin, K., Tang, D., Wang, C., Sakyi, P.A., 2016. LA-ICP-MS U–Pb zircon, columbite-tantalite and ^{40}Ar–^{39}Ar muscovite age constraints for the rare-element pegmatite dykes in the Altai orogenic belt, NW China. Geological Magazine 155, 707-728.

Zhu, X.K., O'Nions, R.K., Gibb, A.J., 1998. SIMS analysis of U–Pb isotopes in monazite: matrix effects. Chemical geology 144, 305-312.

Zhu, Z.Y., Wang, R.C., Che, X.D., Zhu, J.C., Wei, X.L., Huang, X.E., 2015. Magmatic–hydrothermal rare-element mineralization in the Songshugang granite (northeastern Jiangxi, China): Insights from an electron-microprobe study of Nb–Ta–Zr minerals. Ore Geology Reviews 65, 749-760.

Figure and table captions

Figure 1: Electron Micro-Probe Analysis of columbite-tantalite samples plotted in the four quadrant Ta/(Nb+Ta) vs. Mn/(Mn+Fe) columbite-tantalite diagram.

Figure 2: ID-TIMS concordia diagrams for the four columbite-tantalite samples from the Ivory Coast dated. (A) Six fragments from the CT1 ferrotapiolite sample yield an age of 2046.8 ± 1.1 Ma (2σ). (B) Six fragments from the CT3 ferrotapiolite sample yield an age of 2053.2 ± 1.3 Ma (2σ). (C) Five fragments from the CT4 ferrotapiolite sample yield an age of 2044.5 ± 1.6 Ma (2σ). (D) Five fragments from the ISSIA2 ferrotapiolite sample present scattered data linked to metamictization, with an age of 2002 ± 32 Ma (2σ).

Figure 3: ID-TIMS concordia diagrams for six samples of columbite-tantalites from Rwanda, China and France. (A) Four fragments from the Rongi ferrocolumbite sample yield an age of 931.5 ± 2.5 Ma (2σ). (B) Four fragments from the Buranga ferrocolumbite sample yield an age of 905.2 ± 3.2 Ma (2σ). (C) Six fragments from the NT-2 ferrotantalite sample yield an age of 372.0 ± 2.3 Ma (2σ). (D) Three fragments from the A-1 ferrotantalite sample yield an age of 198.3 ± 1.4 Ma (2σ). Several fragments present scattered Pb/U isotopic values, linked to metamictization and/or nano-inclusions. (E) Six fragments from the NP2 ferrotantalite sample yield an age of 380.3 ± 2.4 Ma (2σ). Several fragments present scattered Pb/U isotopic values, linked to metamictization and/or nano-inclusions. (F) Four fragments from the CC1716 ferrocolumbite sample yield an age of 326.3 ± 0.6 Ma (2σ). Several fragments present scattered Pb/U isotopic values, linked to metamictization and/or nano-inclusions

Figure 4: Binary diagrams from SIMS measurements. (A) $^{206}Pb/^{238}U$ vs UO/U of measured samples according to their chemical composition. Each group of chemical composition is defined by a linear relation corresponding to the SIMS calibration line. This line depends on the composition and age of each sample. (B) $[^{206}Pb/^{238}U_{SIMS}]/[^{206}Pb/^{238}U_{ID-TIMS}]$ vs UO/U. The effect of the age of each sample is compensated by the use of ID-TIMS age. This diagram demonstrates that the different chemical composition of the tested columbite-tantalite samples induce matrix effect during SIMS measurements. Note, the ferrotapiolite sample from Rongi does not fall on the common trend due to the difference between ID-TIMS and SIMS ages. See text for details.

Figure 5: Binary diagrams plotting $[^{206}Pb/^{238}U_{SIMS}]/[^{206}Pb/^{238}U_{ID-TIMS}]$ ratios against Ta# and Mn# (calculated from SIMS and EPMA measurements). Ta# and Mn# reflect the two main chemical substitutions in columbite-tantalite minerals. These diagrams demonstrate that linear matrix effect by SIMS is only linked to the Ta#, whereas the Mn# has almost no impact. Note, the significant substitution of Ti, Sc, W, and/or Sn will disturb the linear trend of the matrix effect as a function of Ta#.

Figure 6: Influence of the matrix effect on the SIMS age calculations. (A) and (B): Concordia diagrams for CT3 Ferrotapiolite calculated with CT1 (matrix-matched) or Buranga (non-matrix-matched) as external standards. (C) Diagram showing the deviation of the SIMS $^{206}Pb/^{238}U$ and $^{207}Pb/^{206}Pb$ ratios versus TIMS $^{206}Pb/^{238}U$ and $^{207}Pb/^{206}Pb$ ratios for the CT3 sample, using a matrix-matched (blue, CT1) and non-matrix-matched (red, Buranga) conditions. (D) Binary diagram illustrating the deviation of the SIMS $^{206}Pb/^{238}U$ ratio versus TIMS $^{206}Pb/^{238}U$ ratio for ferrocolumbite CC1716, using three

standards of different Ta#: CT1 (ferrotapiolite), NP2 (ferrotantalite) and Buranga (ferrocolumbite).

Figure 7: SIMS age calculations for the different columbite-tantalite samples from this study, in matrix-matched conditions. (A) and (B): Concordia diagrams for two samples of Ferrotapiolite CT3 and CT4 calculated with CT1 as external standard. (A) Thirty measurements of the CT3 ferrotapiolite sample yield an age of 2054.1 ± 2.2 Ma (2σ). (B) Nine measurements of the CT4 ferrotapiolite sample yield an age of 2042.0 ± 4.0 Ma (2σ). (C) and (D) Concordia diagrams for two samples of Ferrocolumbite Rongi and CC1716 calculated with Buranga as external standard. (C) Seventeen measurements of the Rongi ferrocolumbite sample yield an age of 905.0 ± 5.0 Ma (2σ). (D) Fourteen measurements of the CC1716 ferrocolumbite sample yield an age of 334.6 ± 2.6 Ma (2σ). (E) Concordia diagram of the NT-2 Ferrotantalite calculated with NP2 as external standard and twenty measurements yielding an age of 372.0 ± 5.8 Ma (2σ), see Figure 8 for more details.

Figure 8: SIMS calculations for the NT-2 ferrotantalite sample calculated with the NP2 ferrotantalite as external standard (twenty measurements). (A) Concordia diagram presenting data corrected for common lead contribution (red) and uncorrected for common lead (black). (B) Terra-Wasserburg plot of the NT-2 sample, yielding an age of 372.0 ± 5.8 Ma (2σ). (C) $^{206}Pb/^{238}U$ individual and mean ages calculated based on data corrected for common lead contribution (red) and uncorrected for common lead contribution (black). (D) $^{207}Pb/^{235}U$ individual and mean ages calculated based on data corrected for common lead contribution (red) and uncorrected for common lead contribution (black).

Table 1: Representative EPMA analyses for columbite-tantalites. Values preceeded by the symbol "<" indicate element concentrations below the detection limit.

Table 2: U-Pb ID-TIMS analytical results for columbite-tantalites.

Table 3: Summary of calculated ID-TIMS and SIMS ages and respective precisions and accuracies

Table 1

	CT1	CT3	CT4	Rongi	Buranga	NP2	NT-2	A-1	ISSIA2	CC1716
TiO_2	0.79	0.71	0.95	0.17	0.77	0.37	0.22	0.38	0.24	1.76
MnO	0.73	0.97	0.62	6.84	9.78	6.54	6.88	14.3	9.72	6.11
FeO	14.8	14.5	14.8	13.8	11.1	10.5	11.6	2.87	6.46	15.4
Nb_2O_5	7.19	6.44	7.51	66.2	64.7	42.7	43.6	27.7	18.4	70.5
SnO_2	<0.2	<0.2	<0.2	<0.2	0.44	0.51	0.28	<0.2	<0.2	<0.2
ZrO_2	<0.2	<0.2	0.21	<0.2	0.31	<0.2	<0.2	<0.2	<0.2	<0.2
Ta_2O_5	75.2	76.2	75.1	11.5	11.9	38.1	37.5	54.6	63.3	6.50
Total	98.94	98.91	99.17	98.66	99.12	98.69	100.1	99.86	98.39	100.3
Structural formula calculated on the basis of O = 6 atoms										
Ti	0.02	0.01	0.02	0.00	0.02	0.01	0.00	0.01	0.00	0.04
Mn	0.02	0.02	0.02	0.20	0.29	0.18	0.19	0.38	0.26	0.18
Fe	0.38	0.37	0.38	0.41	0.33	0.29	0.32	0.08	0.17	0.46
Nb	0.17	0.15	0.17	1.78	1.74	1.07	1.09	0.67	0.44	1.90
Sn	0.00	0.00	0.00	0.00	0.01	0.01	0.01	0.01	0.00	0.00
Zr	0.00	0.01	0.01	0.00	0.01	0.00	0.00	0.00	0.00	0.00
Ta	2.06	2.08	2.05	0.36	0.38	1.12	1.10	1.54	1.78	0.21
Mn#	0.05	0.06	0.04	0.33	0.47	0.38	0.37	0.83	0.60	0.28
Ta#	0.92	0.93	0.92	0.17	0.18	0.51	0.50	0.70	0.80	0.10

Mn# = Mn/(Fe+Mn) (atomic ratios)
Ta# = Ta/(Nb+Ta) (atomic ratios)

Table 2

Sample [a]	Weight (mg)	Concentrations (ppm)		$^{206}Pb/^{204}Pb$ Measured ratios [b]	Common lead (pg)	Radiogenic Pb (at%) [c]			Th/U [d]	Atomic ratios [c]							Apparent ages (Ma) [e]		
		U	Pb			^{206}Pb	^{207}Pb	^{208}Pb		$^{206}Pb/^{238}U$	Err (2σ) %	$^{207}Pb/^{235}U$	Err (2σ) %	$^{207}Pb/^{206}Pb$	Err (2σ) %	Error corr	$^{206}Pb/^{238}U$	$^{207}Pb/^{235}U$	$^{207}Pb/^{206}Pb$
CT1, Ivory Coast, Ferrotapiolite *(common lead: $^{206}Pb/^{204}Pb$ = 15.3 , $^{207}Pb/^{204}Pb$ = 15.3, $^{208}Pb/^{204}Pb$ = 35)*																			
1	0.200	181	70.5	1100	13500	88.55	11.16	0.282	0.0100	.38121	0.64	6.6273	0.66	0.12609	0.14	0.9774	2082	2063	2044
2	0.210	201	73.3	33700	17	88.76	11.23	0.004	0.0001	.37597	0.53	6.5594	0.53	0.12654	0.04	0.9965	2057	2054	2050
3	0.292	200	72.8	47700	8	88.80	11.20	0.002	0.0001	.37590	0.62	6.5406	0.61	0.12620	0.05	0.9970	2057	2051	2046
4	*0.213*	*202*	*314*	*38.84*	*4670000*	*-f*	*-f*	*-f*											
5	0.267	191	70.1	13200	99	88.76	11.21	0.034	0.0012	.37699	1.08	6.5638	1.08	0.12628	0.07	0.9977	2062	2054	2047
6	0.560	194	71.1	23890	31	88.79	11.20	0.009	0.0004	.37691	0.84	6.5584	0.84	0.12620	0.05	0.9985	2062	2054	2046
7	0.585	208	77.4	1770	6400	88.65	11.19	0.158	0.0056	.37046	1.03	6.4493	1.06	0.12626	0.16	0.9890	2032	2039	2046
CT3, Ivory Coast, Ferrotapiolite *(common lead: $^{206}Pb/^{204}Pb$ = 15.3 , $^{207}Pb/^{204}Pb$ = 15.3, $^{208}Pb/^{204}Pb$ = 35)*																			
8	0.306	309	113	49100	19	88.75	11.24	0.005	0.0002	.37658	0.61	6.5786	0.61	0.12670	0.04	0.9983	2060	2057	2053
9	0.458	321	118	83700	7	88.73	11.26	0.005	0.0002	.38039	0.56	6.6558	0.56	0.12690	0.03	0.9984	2078	2067	2056
10	0.504	304	111	65000	10	88.76	11.24	0.002	0.0001	.37660	0.68	6.5769	0.68	0.12666	0.05	0.9976	2060	2056	2052
11	0.182	312	113	14100	226	88.73	11.25	0.230	0.0008	.37559	0.73	6.5659	0.73	0.12679	0.04	0.9987	2056	2055	2054
12	0.158	306	114	2770	5740	88.66	11.22	0.118	0.0042	.37484	0.77	6.5431	0.77	0.12660	0.05	0.9978	2052	2052	2051
13	0.212	294	107	11900	286	88.74	11.23	0.290	0.0010	.37406	0.58	6.5244	0.58	0.12650	0.04	0.9975	2049	2049	2050
CT4, Ivory Coast, Ferrotapiolite *(common lead: $^{206}Pb/^{204}Pb$ = 15.3 , $^{207}Pb/^{204}Pb$ = 15.3, $^{208}Pb/^{204}Pb$ = 35)*																			
14	0.376	181	68.2	909	18000	88.51	11.14	0.349	0.0124	.36418	0.65	6.3222	0.66	0.12591	0.11	0.9866	2002	2022	2042
15	0.141	169	62.3	3360	1180	88.73	11.17	0.910	0.0032	.37330	0.40	6.4817	0.40	0.12593	0.05	0.9920	2045	2043	2042
16	0.168	176	63.9	11100	116	88.78	11.19	0.230	0.0008	.37365	0.57	6.4946	0.57	0.12606	0.10	0.9834	2047	2045	2044
17	0.189	177	65.1	4010	924	89.47	11.29	0.761	0.0267	.37763	0.59	6.5722	0.59	0.12622	0.07	0.9919	2065	2056	2046
18	0.238	175	64.4	8190	216	88.77	11.19	0.034	0.0012	.37778	0.43	6.5688	0.43	0.12611	0.10	0.9708	2066	2055	2044
Rongi, Rwanda, Ferrocolumbite *(common lead: $^{206}Pb/^{204}Pb$ = 17.5 , $^{207}Pb/^{204}Pb$ = 15.5, $^{208}Pb/^{204}Pb$ = 37.0)*																			
19	*0.227*	*59.5*	*8.25*	*1090*	*275*	*93.54*	*6.433*	*0.031*	*0.0010*	*.14127*	*0.66*	*1.33961*	*0.76*	*0.06877*	*0.04*	*0.8678*	*852*	*863*	*892*
20	*0.239*	*74.0*	*236*	*22.10*	*5416000*	*-g*	*-g*	*-g*											
21	0.122	99.8	14.8	1710	367	93.40	6.561	0.040	0.0013	.15422	0.63	1.49381	0.70	00.07025	0.32	0.8915	925	928	936
22	*0.112*	*91.4*	*27.8*	*83.04*	*225000*	*92.64*	*6.845*	*0.519*	*0.0173*	*.15152*	*0.84*	*1.54364*	*2.63*	*0.07389*	*2.48*	*0.33*	*910*	*948*	*1038*
23	0.231	74.2	11.3	862	275	93.43	6.555	0.017	0.0005	.15294	1.18	1.47956	1.27	0.07016	0.44	0.9382	917	922	933
24	0.308	85.4	14.8	328	8000	93.25	6.576	0.171	0.0057	.15263	2.09	1.48410	2.12	0.07052	0.32	0.9885	916	924	944
25	*0.210*	*77.6*	*26.1*	*68.37*	*249000*	*91.99*	*6.607*	*1.407*	*0.0476*	*.14271*	*1.15*	*1.41333*	*2.16*	*0.07183*	*1.90*	*0.47*	*860*	*895*	*981*
26	0.231	80.5	11.8	2740	94	93.41	6.548	0.040	0.0013	.15559	0.72	1.50388	0.73	0.07010	0.13	0.9836	932	932	931
NP2, Fujian, China, Ferrocolumbite *(common lead: $^{206}Pb/^{204}Pb$ = 18.6, $^{207}Pb/^{204}Pb$ = 15.6, $^{208}Pb/^{204}Pb$ = 37.5)*																			
27	0.216	248	14.7	904	1130	94.78	5.141	0.080	0.0026	.06032	0.60	0.45112	0.77	0.05424	0.47	0.7888	378	378	381

28	0.194	272	16.2	716	2160	94.84	5.121	0.040	0.0013	.06003	0.65	0.44693	1.68	0.05399	1.54	0.40	376	375	371
29	*0.295*	*211*	*12.0*	*1010*	*615*	*95.37*	*5.029*	*0.399*	*0.0131*	*.05865*	*1.10*	*0.42643*	*7.23*	*0.05273*	*7.13*	*0.18*	*367*	*361*	*317*
30	0.316	136	12.3	1730	229	94.83	5.136	0.030	0.0010	.09566	1.05	0.71432	1.07	0.05416	0.21	0.9800	589	547	378
31	0.271	322	15.6	1310	634	94.83	5.128	0.040	0.0013	.05085	0.78	0.37916	0.89	0.05408	0.42	0.8800	320	326	374
32	*0.193*	*235*	*14.3*	*730*	*1600*	*94.64*	*5.195*	*0.164*	*0.0051*	*.06089*	*0.64*	*0.46079*	*0.73*	*0.05489*	*0.34*	*0.8831*	*381*	*385*	*408*
33	0.206	276	15.9	1220	751	94.77	5.139	0.092	0.0028	.05999	0.70	0.44852	0.72	0.05423	0.16	0.9757	376	376	380
34	0.201	241	13.9	1390	446	94.78	5.145	0.075	0.0026	.06052	0.71	0.45300	0.74	0.05428	0.22	0.9558	379	379	383

Buranga, Rwanda, Ferrocolumbite (common lead: $^{206}Pb/^{204}Pb$ = 17.5 , $^{207}Pb/^{204}Pb$ = 15.5, $^{208}Pb/^{204}Pb$ = 37.0)

35	0.234	84.4	12.1	1610	278	93.49	6.480	0.025	0.0010	.14946	0.71	1.42838	0.86	0.06931	0.49	0.8254	898	901	908
36	*0.196*	*163*	*76.5*	*48.22*	*310400*	*91.66*	*6.503*	*1.835*	*0.0058*	*.13569*	*1.73*	*1.32727*	*3.97*	*0.07095*	*3.73*	*0.35*	*820*	*858*	*956*
37	0.232	80.3	11.3	5350	23	93.54	6.457	0.001	0.0000	.15135	1.18	1.44057	1.24	0.06903	0.39	0.9500	909	906	900
38	*0.265*	*89.8*	*16.0*	*262*	*13700*	*93.40*	*6.581*	*0.015*	*0.0004*	*.14927*	*1.35*	*1.45021*	*1.58*	*0.07046*	*0.79*	*0.8660*	*870*	*910*	*942*
39	0.348	74.5	10.6	4430	30	93.49	6.475	0.039	0.0013	.15218	1.04	1.45326	1.06	0.06926	0.21	0.9795	913	911	906
40	0.379	67.6	9.49	6450	11	93.46	6.478	0.061	0.0021	.15108	1.16	1.44379	1.18	0.06931	0.18	0.9886	907	907	908
41	0.378	84.0	11.7	7800	11	93.45	6.493	0.056	0.0019	.14442	1.20	1.38367	1.20	0.06949	0.11	0.9959	870	882	913

NT-2, Shanxi, China, Ferrotantalite (common lead: $^{206}Pb/^{204}Pb$ = 18.6 , $^{207}Pb/^{204}Pb$ = 15.6, $^{208}Pb/^{204}Pb$ = 37.5)

42	0.319	218	13.2	534	2380	94.87	5.131	0.002	0.2316	.05885	0.89	0.43878	0.94	0.05408	0.27	0.9571	369	369	374
43	0.243	142	8.86	341	2390	94.80	5.124	0.074	0.3719	.05665	0.82	0.42216	1.02	0.05405	0.56	0.8352	355	358	373
44	0.434	149	9.86	314	3400	94.78	5.136	0.081	0.4052	.05948	1.28	0.44438	1.36	0.05418	0.42	0.9504	373	373	379
45	0.242	154	8.99	713	648	94.84	5.134	0.029	0.1729	.05851	0.98	0.43673	1.04	0.05413	0.31	0.9533	367	368	377
46	*0.208*	*231*	*40.9*	*49.01*	*765000*	*92.90*	*5.122*	*1.979*	*3.8079*	*.06174*	*1.24*	*0.46931*	*3.93*	*0.05514*	*3.77*	*0.28*	*386*	*391*	*418*
47	0.265	174	10.2	923	519	94.81	5.147	0.043	0.0014	.06037	1.63	0.45190	1.63	0.05429	0.15	0.9957	378	379	383
48	0.250	166	10.3	479	1750	94.78	5.174	0.049	0.0016	.05957	0.57	0.44837	0.69	0.05459	0.38	0.8364	373	376	396

A-1, Xinjiang, China, Ferrotantalite (common lead: $^{206}Pb/^{204}Pb$ = 18.6 , $^{207}Pb/^{204}Pb$ = 15.6, $^{208}Pb/^{204}Pb$ = 37.5)

49	0.207	81.3	2.92	274	393	94.88	4.741	0.381	0.0127	.03117	1.24	0.21477	1.68	0.04997	1.07	0.7696	198	198	194
50	0.233	304	9.96	454	1900	95.02	4.758	0.220	0.0073	.03120	1.62	0.21544	1.70	0.05008	0.40	0.9713	198	198	199
51	*0.199*	*78.3*	*15.9*	*1220*	*756*	*95.04*	*4.752*	*0.204*	*0.0067*	*.21185*	*1.96*	*1.46057*	*1.98*	*0.05000*	*0.23*	*0.9934*	*1239*	*914*	*195*
52	*0.199*	*274*	*11.3*	*1530*	*253*	*95.05*	*4.752*	*0.201*	*0.0066*	*.04370*	*0.68*	*0.30122*	*0.70*	*0.05000*	*0.17*	*0.9691*	*276*	*267*	*195*
53	*0.184*	*213*	*13.0*	*305*	*6500*	*95.01*	*4.740*	*0.251*	*0.0083*	*.05436*	*0.70*	*0.37390*	*0.92*	*0.04989*	*0.56*	*0.7979*	*341*	*323*	*190*
54	*0.202*	*42.1*	*17.8*	*1010*	*1400*	*95.04*	*4.750*	*0.206*	*0.0068*	*.04363*	*0.72*	*0.30070*	*0.75*	*0.04998*	*0.18*	*0.9695*	*275*	*267*	*194*
55	0.145	515	16.0	703	2210	95.05	4.765	0.184	0.0061	.03129	1.00	0.21624	1.06	0.05013	0.32	0.9522	199	199	201

ISSIA2, Ivory Coast, Manganocolumbite (common lead: $^{206}Pb/^{204}Pb$ = 15.3 , $^{207}Pb/^{204}Pb$ = 15.3, $^{208}Pb/^{204}Pb$ = 35)

56	0.275	344	21.9	141	49100	87.97	10.82	1.218	0.0433	.04440	0.92	0.75280	1.00	0.12297	0.40	0.9178	280	570	2000
57	0.191	990	469	1290	284000	70.89	8.810	20.29	0.8976	.37592	0.69	6.44125	0.70	0.12427	0.08	0.9936	2057	2038	2018
58	0.204	172	9.61	199	5500	88.44	10.80	0.761	0.0269	.04360	0.87	0.73410	0.92	0.12211	0.30	0.9463	275	559	1987
59	0.200	436	160	1130	66400	88.97	10.84	0.19	0.0067	.36082	1.09	6.06039	1.09	0.12182	0.06	0.9982	1986	1985	1983
60	0.194	575	24.5	634	4600	88.76	10.92	0.319	0.0112	.04013	1.02	0.68079	1.03	0.12303	0.11	0.9946	254	527	2001

CC1716, France, Ferrocolumbite (common lead: $^{206}Pb/^{204}Pb$ = 17.9 , $^{207}Pb/^{204}Pb$ = 15.6, $^{208}Pb/^{204}Pb$ = 38.1)

61	0.151	9.66	24.3	7520	49	94.44	4.999	0.566	0.0188	2.7446	1.10	20.0333	1.10	0.05294	0.07	0.9978	8511	3093	326
62	0.122	262	23.6	9620	28	94.46	5.002	0.541	0.0179	.04996	0.85	0.36473	0.85	0.05295	0.10	0.9937	314	316	327
63	0.126	54500	2523	327000	270	92.11	4.877	3.011	0.1025	.04961	2.51	0.36216	2.51	0.05295	0.03	0.9999	312	314	326
64	0.121	532	30.5	394	22400	94.31	4.995	0.698	0.0232	.05322	0.66	0.38861	0.80	0.05296	0.43	0.8463	334	333	327

| 65 | 0.115 | 14800 | 748 | 1840 | 702000 | 91.75 | 4.853 | 3.402 | 0.1163 | .05185 | 0.85 | 0.37817 | 0.86 | 0.05290 | 0.09 | 0.9943 | 326 | 326 | 324 |

[a]Small fragments from single columbite grains. Fragments were selected to show only fresh fracture surfaces. All samples were leached with 20% HF, 6N HCl, and 7N HNO_3 before sample dissolution (Romer and Smeds, 1996). After leaching, most grains had shinny metallic surfaces no traces of sulphides, silicate inclusions and metamict domains. Rare grains developed rusty stains during the HCl and HNO3 washing stages, indicating that metamict domains were not completely removed. As such grains typically yield variably discordant data, they were removed from the sample. Although the analysed fragments eventually had perfect surfaces, it is unclear whether the metamict domains had been removed completely also from interior part accessible to leaching. To minimize the risk for non-idenified metamict portions, small fragments were selected preferentially for analysis. The high discordance of some samples indicates that this apparently was not always possible to remove all metamict parts.

[b]Lead isotope ratios corrected for fractionation, blank and isotopic tracer. Samples were analysed at GFZ German Research Centre for Geosciences, Potsdam, Germany, using a ^{205}Pb-^{235}U mixed isotopic tracer. Analytical details are given in Baumgartner et al. (2006). During the measurement period total blanks were less than 15 pg, for lead and less than 1 pg for uranium.

[c]Lead corrected for fractionation, blank, isotopic tracer, and initial lead with the composition according to Stacey and Kramers (1975).

[d]^{232}Th/^{238}U calculated from radiogenic ^{208}Pb/^{206}Pb and the age of the sample.

[e]Apparent ages were calculated using the constants recommended by IUGS. λ_{238} = 1.55125 E-10 y^{-1}, λ_{235} = 9.848 E-10 y^{-1}.

[f]Sample dominated by common lead; measured ^{206}Pb/^{204}Pb = 38.84 , ^{207}Pb/^{204}Pb = 18.21, ^{208}Pb/^{204}Pb = 38.89.

[g]Sample dominated by common lead; measured ^{206}Pb/^{204}Pb = 22.10 , ^{207}Pb/^{204}Pb = 15.92, ^{208}Pb/^{204}Pb = 38.91.
Data in italic were removed for age calculation.

Table 3

Sample	Number of ID-TIMS analyses	ID-TIMS calculated age (2σ)	Number of SIMS analyses	Range of precision per analysis ($^{206}Pb/^{238}U$)	Range of precision per analysis ($^{207}Pb/^{206}Pb$)	SIMS calculated concordia age (2σ)	Precision[a]	Accuracy[b]
CT1	6 (7)	2046.8 ± 1.1 Ma	38 (41)	*Standard*	-	-	-	-
CT3	6 (6)	2053.2 ± 1.3 Ma	30 (36)	0.3 – 2.3 %	0.1 - 0.4 %	2054.1 ± 2.2 Ma	0.2 %	99.8 %
CT4	5 (5)	2044.5 ± 1.6 Ma	9 (10)	0.3 – 1.7 %	0.1 – 0.3 %	2042.0 ± 4.0 Ma	0.2 %	99.9 %
Buranga	5 (7)	905.2 ± 2.3 Ma	25 (35)	*Standard*	-	-	-	-
Rongi	4 (8)	931.5 ± 2.5 Ma	17 (17)	0.6 – 2.2 %	1.4 – 6.9 %	905.0 ± 5.0 Ma	0.6 %	[c]
CC1716	5 (5)	326.3 ± 0.6 Ma	14 (15)	0.6 – 1.2 %	3.5 – 21.4 %	334.6 ± 2.6 Ma	0.6 %	97.9 %
NP2	6 (8)	380.3 ± 2.4 Ma	24 (24)	*Standard*	-	-	-	-
NT-2	6 (7)	372.0 ± 2.3 Ma	18 (21)	0.8 – 3.1 %	4.9 – 58.4 %	371.3 ± 3.7* Ma	1.5 %	100 %
A-1	3 (7)	198.3 ± 1.4 Ma	(5)	-	-	-	-	-

[a] Calculated from SIMS calculated ages
[b] Calculated deviation between ID-TIMS and SIMS calculated concordia ages
*: mean $^{206}Pb/^{238}U$ age used
Numbers of analyses are given as follow: Number of analyses used for calculation (Total number of analyses)
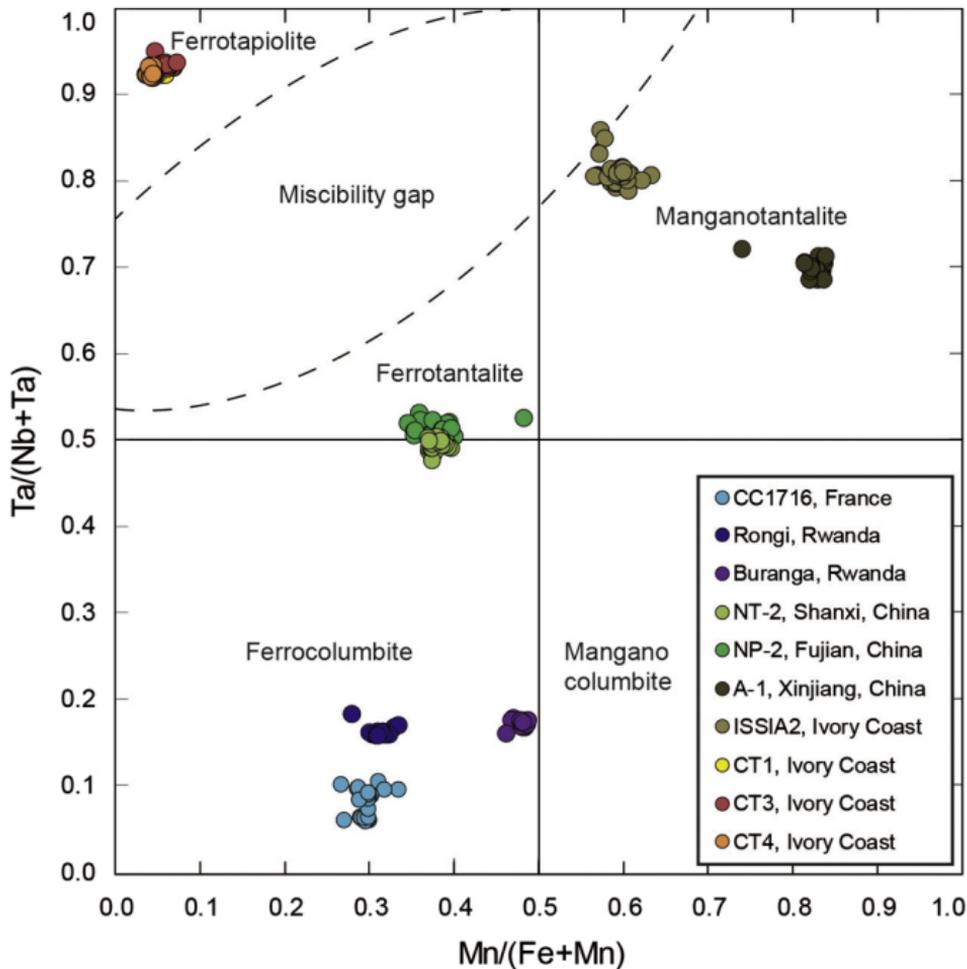
Figure 1
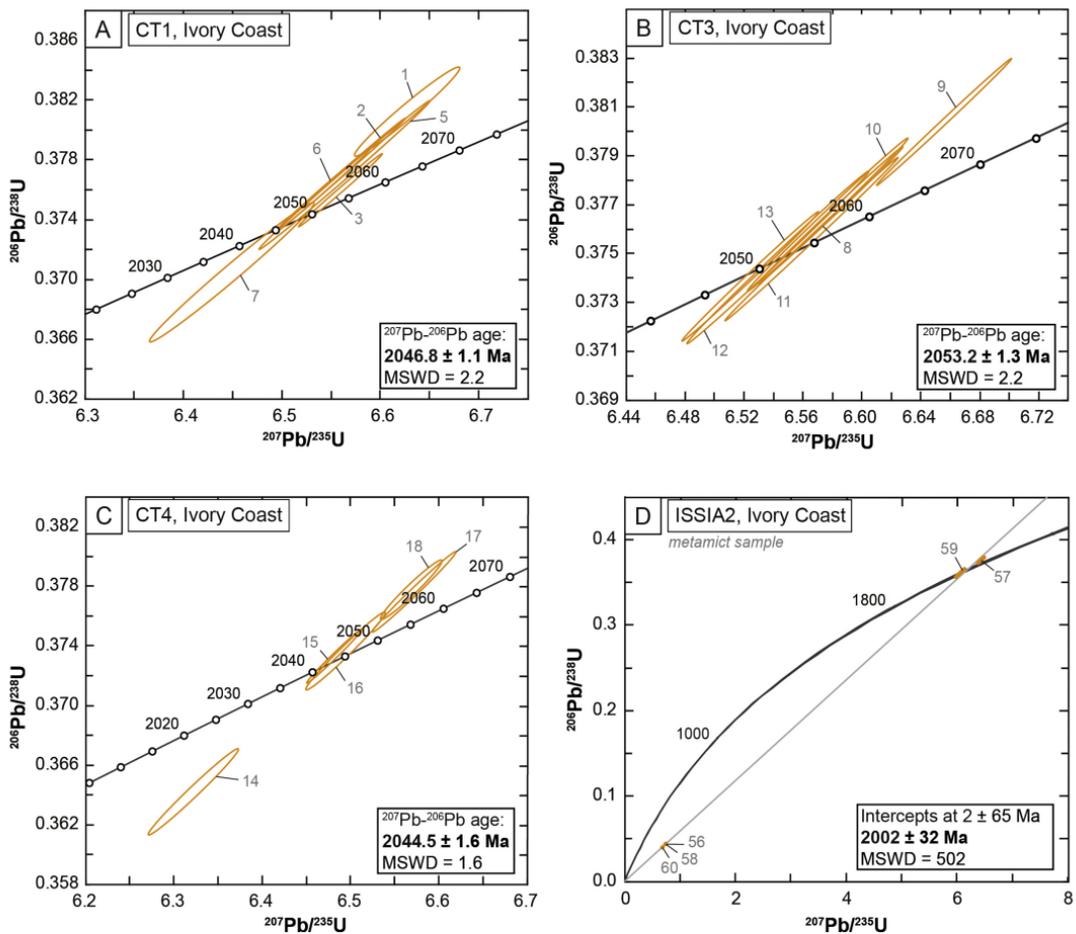
Figure 2
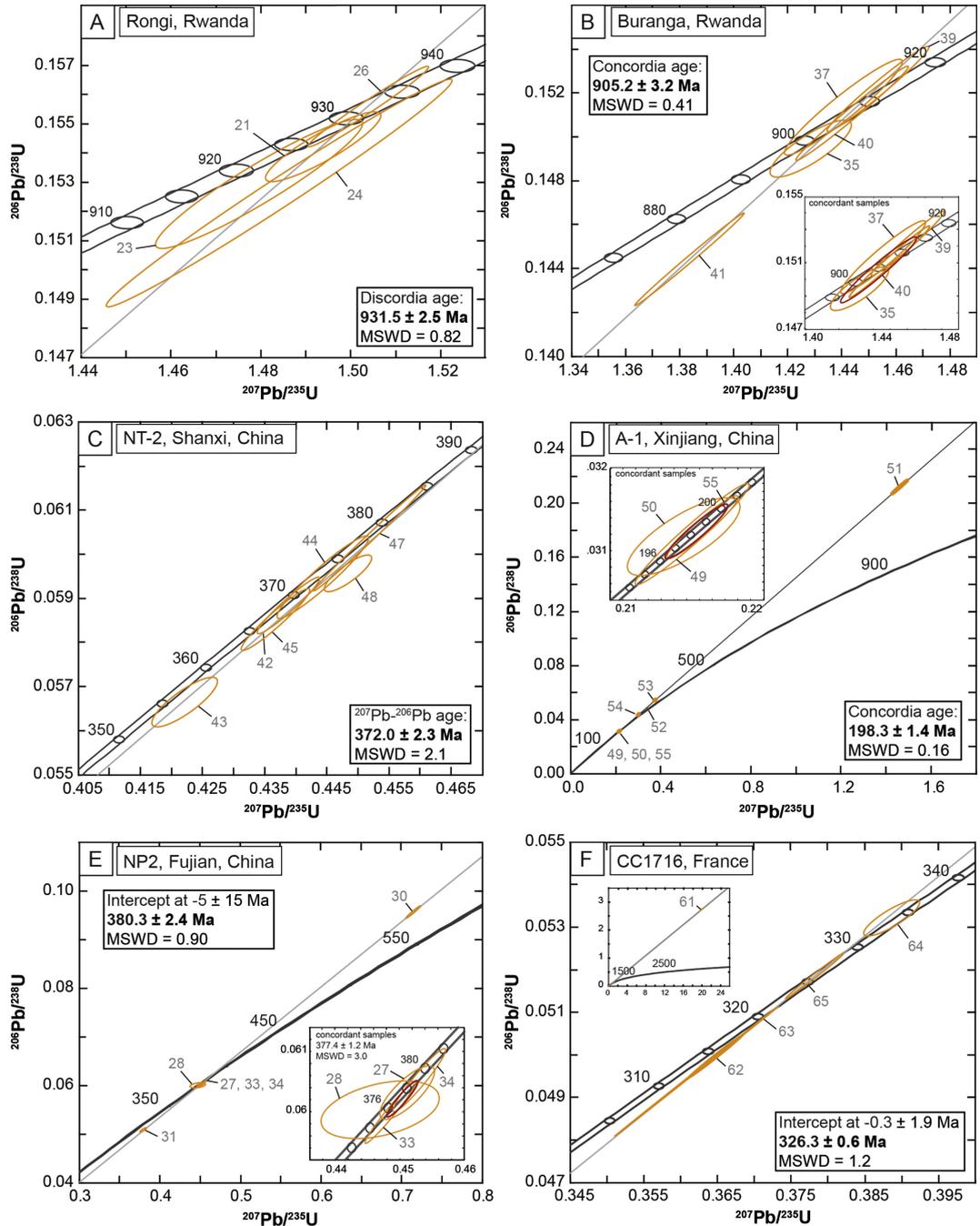
Figure 3
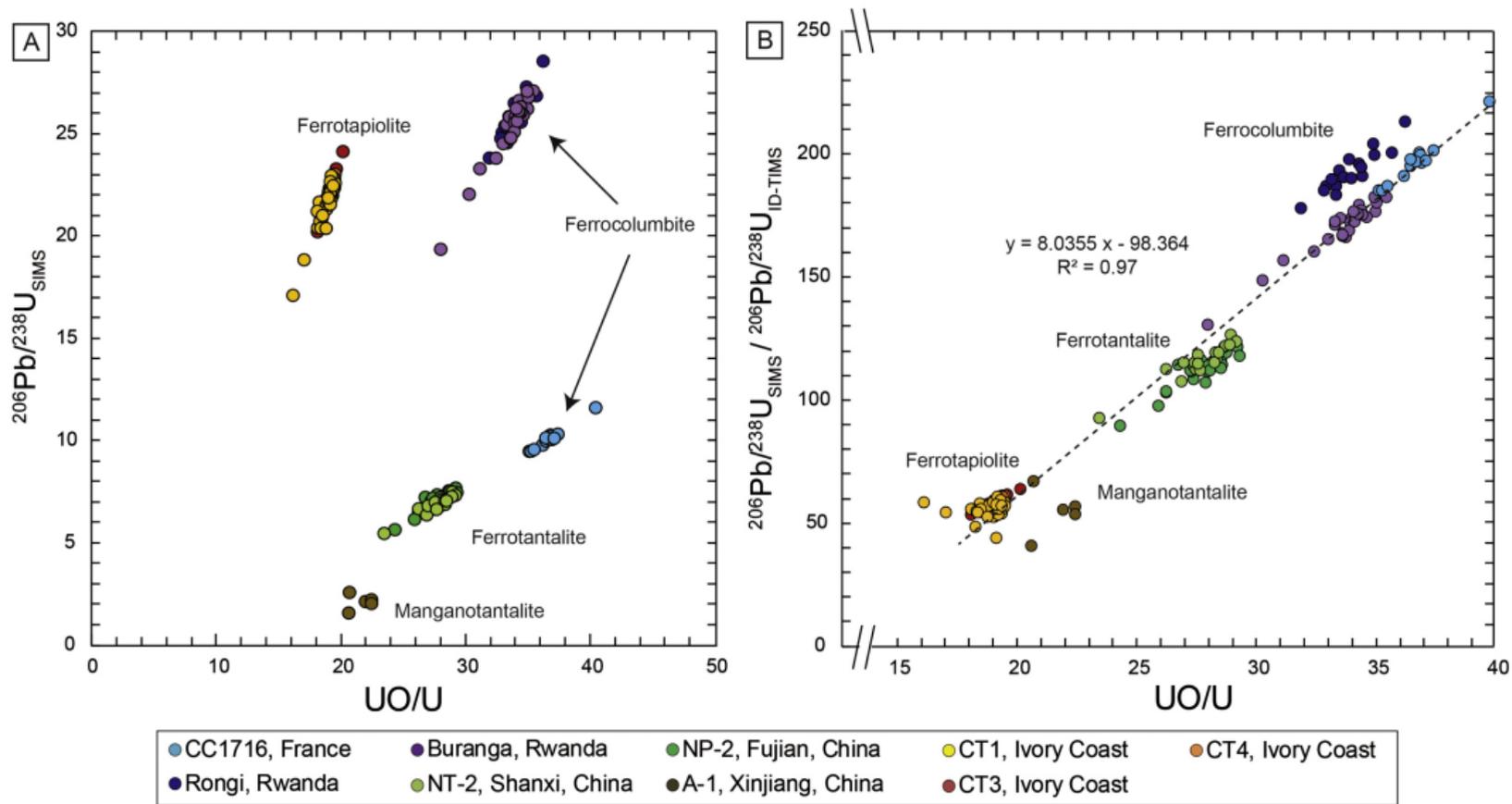
Figure 4
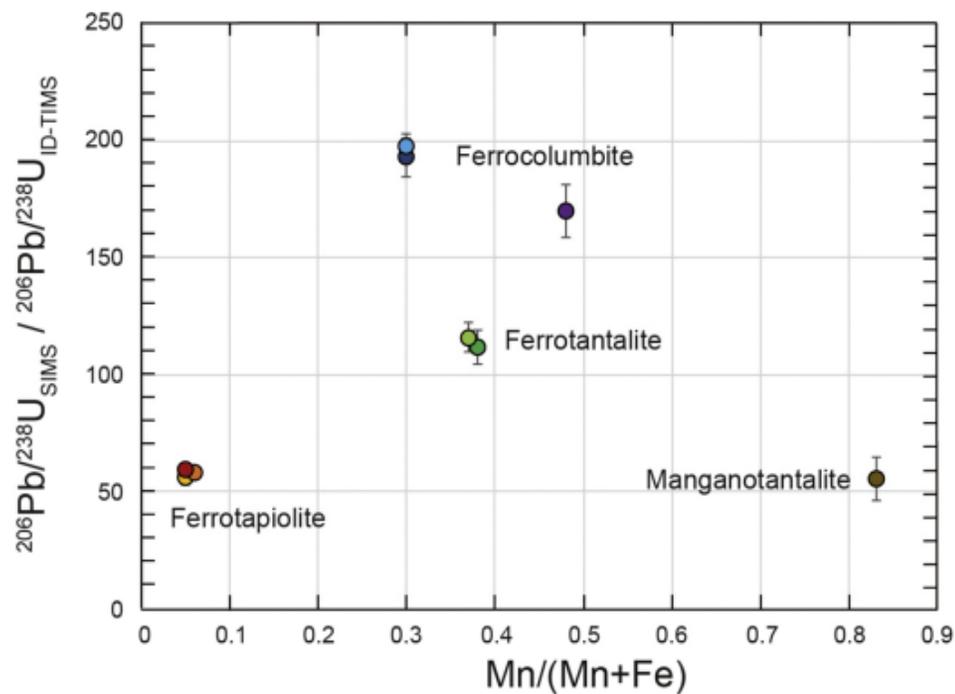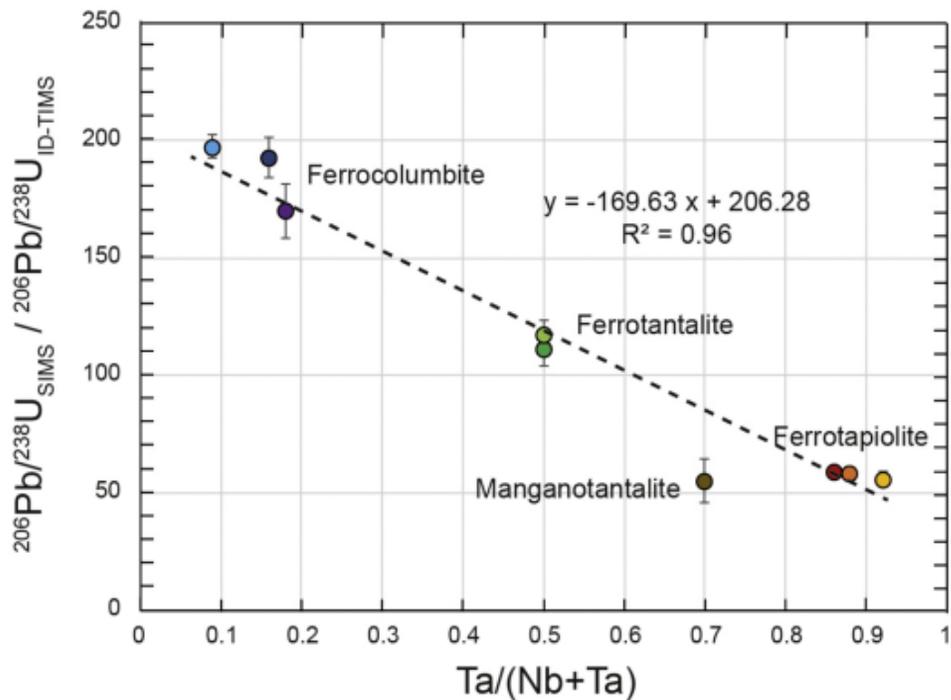
Figure 5
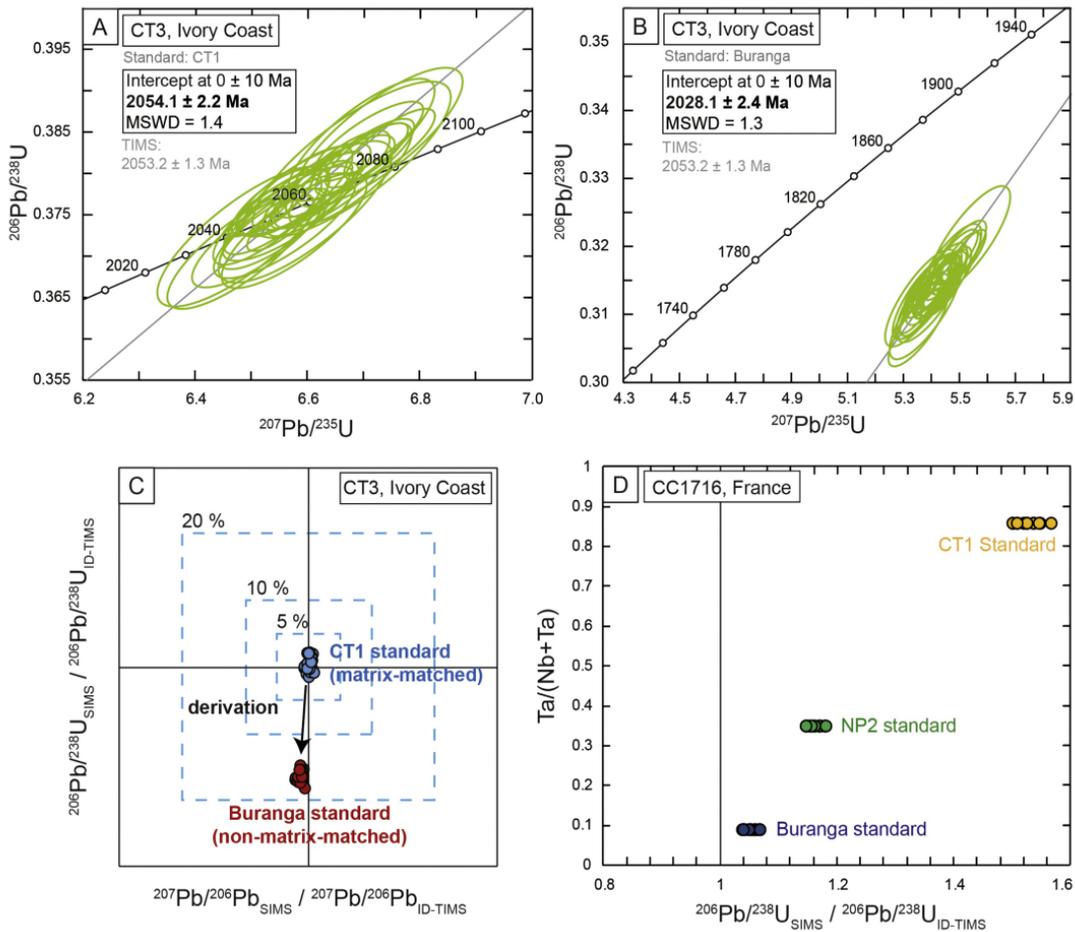
Figure 6

Figure 7

Figure 8